SMART IMAGE-GUIDED NEEDLE INSERTION

FOR TISSUE BIOPSY

A THESIS SUBMITTED TO THE GRADUATE DIVISION OF THE
UNIVERSITY OF HAWAIʻI AT MĀNOA IN PARTIAL FULFILLMENT
OF THE REQUIREMENTS FOR THE DEGREE OF

MASTER OF SCIENCE

IN

MECHANICAL ENGINEERING

DECEMBER 2019

By

Zahra Khashei Varnamkhasti

Thesis Committee:

Bardia Konh, Chairperson
Mehrdad Ghasemi-Nejhad
Peter Berkelman
Zachary Trimble

Keywords: Needle Insertion, Image-Guided, Biopsy

ACKNOWLEDGMENTS

I would like to thank many people at University of Hawaii at Manoa who helped and supported me. First and foremost, I would like to appreciate my advisor, Dr. Bardia Konh, who gave me the opportunity to work in his active research team and supported me during my graduate studies. His supports and motivations kept me going despite of eventual failures and made me interested to research new fields. I would like to thank my Thesis Committee Members, Dr. Mehrdad Ghasemi Nejhad, Dr. Zachary Trimble, and Dr. Peter Berkelman for all their help and support. This work was financially supported by Hawaii Community Foundation, Grant ID # 18ADVC-90805, that I am grateful for.

ABSTRACT

Motivation: Various needle-based procedures have been practiced in cancer interventions in recent years. Needle insertion as one of the most popular techniques could facilitate minimally invasive surgeries such as biopsy and brachytherapy to extract or kill the cancer locally, respectively. Needle insertion process may become more challenging and complicated due to several difficulties in needle navigation and targeting accuracy. To resolve this issue and for effective control during the needle insertion tasks, active flexible needles are proposed in this work to replace passive rigid needles in medical practice. Utilizing active needles in minimally invasive procedures enhances the needles' maneuverability under actuation forces, and thereby facilitates needle steering within the biological tissue. This work presents three novel active needle designs to enable needle deflection in three directions. Needle steering is visualized and tracked via an imaging system with a 2D transducer connected to an ultrasound machine positioned on the tissue surface. Needle insertion and ultrasound probe displacement are automatically operated.

Methods: The design of the three steerable active needles and the fabrication process are discussed. The active needles are tested in air and in a tissue-mimicking phantom. A motorized system is developed to control the needle insertion, via axial movement and rotation of the needle, and planar movement of the ultrasound transducer. An ultrasound image-guided procedure to visualize and track the needle tip inside a tissue-mimicking phantom in order to reaching target location is fully described. The phantom preparation based on a low-cost and high-quality experimental method is explained as well.

Result: Three active needles were designed, fabricated, and tested in air and tissue-mimicking phantom to realize angular deflection of needle tip in three-dimensional directions. All needles were modeled in SOLIDWORKS. A setup was developed to pull the wires with three programmable stepper motors. To show the needle deflection in air, two cameras were positioned to capture and record top and side views for angular deflection. Tracking was also done by an ultrasound probe when the needle is inserted in tissue. Furthermore, an insertion setup was developed to simultaneously control needle insertion and rotation (if needed). The setup includes a motorized stage attached to the ultrasound probe for planar movement to allow needle tip tracking and guidance inside the tissue. The probe was placed perpendicular to the tissue surface and was attached to a Doppler ultrasound machine. Captured images were transferred to a

computer for analysis. Experimental observations validate a reasonable amount of needle angular deflection equal to 11.49° and 11.06° in air and tissue, respectively.

Conclusion: This experimental study demonstrated the capability of three novel active flexible needles to steer inside the tissue via control and actuation. Needle navigation was improved via enhanced flexibility of the active needles and their active 3D deflection. Needle tracking was also improved via utilization of an ultrasound imaging device. The modulus of the needle insertion system developed in this work is expected to assist in precise needle placement at target positions via a curvilinear approach, while avoiding anatomical obstacles. This approach is also advantageous in minimally invasive procedures such as lumpectomy, biopsy and brachytherapy.

TABLE OF CONTENTS

LIST OF TABLES

LIST OF FIGURES

LIST OF ABBREVIATIONS

FNA	Fine Needle Aspirate
CNB	Core Needle Biopsy
MRI	Magnetic Resonance Imaging
US	Ultrasound
MDR	Markov Decision Process
DP	Dynamic Programming
SMR	Stochastic Motion Roadmap
FBG	Fiber Bragg Grating
SMA	Shape Memory Alloy
SME	Shape Memory Effect
Ni-Ti	Nickel-Titanium
TUSS	Tracked Ultrasound Snapshot
RANSAC	Random Sample Consensus
TRUS	Transrectal Ultrasound
FPS	Frames Per Second
GN	Gain
PWR	Power
FRQ	Factor Represents Frequency
DN	Dynamic
D	Depth
PDMS	Polydimethylsiloxane
SLIC	Simple Linear Iterative Clustering
ID	Inner Diameter
OD	Outer Diameter
2D	Two-Dimensional
3D	Three-Dimensional

LIST OF SYMBOLS

σ	Stress
ε	Strain
T	Temperature
ζ	Martensite volume fraction
ξ_s	Stress-induced fraction
ξ_T	Temperature-induced fraction
σ_0	Initial stress
ε_0	Initial strain
ξ_0	Initial martensite volume fraction
T_0	Initial temperature
Θ	Thermoelastic coefficient
Ω	Phase transformation coefficient
E	Modulus of elasticity
ε_L	Maximum recoverable strain
M_f	Martensite finish
M_s	Martensite start
A_s	Austenite start
A_f	Austenite finish
σ_s^{cr}	Critical start stress
σ_f^{cr}	Critical finish stress
C_A	Stress-influence coefficient of austenite
C_M	Stress-influence coefficient of martensite
a_A	Material constant in austenite phase
a_M	Material constant in martensite phase
D	Diameter
d	Displacement
s	Step
A	Area
F	Force
m	Mass
r	Motor shaft radius
τ	Torque

R_r	Rear radius of curvature
R_f	Front radius of curvature
R_α	Needle tip radius of curvature
L	Length
φ	Angular deflection at the end of insertion
α	Angular deflection at the beginning of insertion

Chapter 1. INTRODUCTION

Surgical tools development has been on the forefront of research studies in recent years to facilitate surgeries for doctors and physicians. The development of new surgical needles has been under investigations to assist surgeons in precise placement of the needle at the target position. This chapter describes needle design and fabrication that can enhance needle-based procedures. Furthermore, the significance of image-guided needle insertion system to track and navigate needle tip is discussed.

1.1. Significance of needle-based procedures in cancer interventions and diagnosis such as brachytherapy and breast cancer biopsy

For decades, cancer has been rated as the second leading cause of death after heart disease in the United States of America as it comprises around 21.7% of total death [1]. Globally recognized [1], about 1 in 6 deaths is due to cancer and approximately, around 70% of that occurs in low- and middle-income countries. Cancer is the result of a rapid and uncontrolled growth of abnormal cells in the human body and it describes a range of diseases that may affect different organs and parts of the body. Usually, normal cells transformation into tumor cells in a multistage process increases the risk of cancer. There are more than 100 detected types of cancer, but the most common ones based on National Cancer Institute [2] reported in 2019 are breast cancer and prostate cancer with the greatest frequency in the United States.

Breast cancer with 271,270 new cases [3] and prostate cancer with 174,650 new cases [4] are listed as common cancer types. Breast cancer originates in the breast tissue when cells start growing out of control. Breast cancer cells often form a tumor, which mostly occurs in women, but men rarely might get that as well. Versus breast cancer in women, the most common and frequently diagnosed cancer in men is prostate cancer that usually happens in older men. Prostate cancer begins in the prostate, a walnut-sized gland in men, and grows very slow where it may not cause serious harm and it could have no signs or symptoms at its early stage.

Cancer has been developed over several years because of different factors both inside and outside of the body. Environmental impact accounts almost two-thirds of all cancer cases in the United States that occurs due to a wide variety of natural and man-made substances. The outside factor includes lifestyle choices that might put human health at a high level of risk to get certain viruses. The significance of environmental factors could be investigated much better when people immigrate to other countries or continents. For instance, Asia is listed as a low risk place for prostate and breast cancer, but high rates of stomach cancer. If Asians move to the United States of America, their prostate and breast cancer rates increase over time and stomach cancer rates decrease. Therefore, lifestyle habits such as diet and exercise, play an important role in the trends for breast and prostate cancers. Some other factors inside the body could lead to rising cancer risk. The most effective risk factors listed in this category are age, race, family history, genes, and obesity. Age is the most effective factor for cancer. The cancer rises significantly after age 50 as

the National Cancer Institute [1] reported that around 25% of new cancer cases are diagnosed in people between 65-74 years old. In addition, race plays a major role to arise cancer development in some people. For example, prostate cancer is more probable to progress in black men compared to other races. Based on the family history of genes, cancer risk may be enhanced if there have been other individuals in the family who struggled with a cancer disease. Obesity is another factor which may cause DNA damage that leads to cancer. Overweight and obese people in comparison with normal-weight people are more likely to face conditions or disorders that are linked to risk factors for certain cancer types.

Considering the above discussion, the importance of cancer treatment has brought attention to firstly achieve cure and secondly palliation where cure is not possible because of an advanced stage of the disease. Once cancer is diagnosed, the patient may need medical treatment and specialized care for months or years. Depending on the tumor grade and location and the stage of the disease, different therapies such as surgery, chemotherapy, radiation therapy, hormonal therapy, targeted therapy and synthetic lethality might be used to treat the cancer. Furthermore, there are several experimental cancer treatments under development.

The main goal of cancer treatment study is to remove the cancer cell completely with minimal damage to the other parts of the patient's body. This reveals the significance of precise cancer diagnosis. Different cancer-related surgical procedures may be practiced, sometimes in combination with other types of interventions. Breast and prostate cancer surgeries have specifically been studied in recent years.

Several surgical procedures including new technologies to remove or treat the cancer are proposed by surgeons and medical researchers to provide aggressive treatment for patients. Today, one significantly applied method is known as minimally invasive surgical procedure, which leaves small incisions with decreased healing time, associated pain and risk of infection. Compared to open surgeries, the minimally invasive procedures allow surgeons to utilize new techniques to make small cuts into the patient's skin and pass tiny tools, illuminations and cameras to perform a surgical task percutaneously. Minimally invasive surgeries could be done by robotic assistance with precise control during a surgical operation, or manually without any robotic assistance.

Among the minimally invasive methods, needle-based surgical procedures are widely known for diagnostic and therapeutic purposes such as biopsy, thermal ablation, and brachytherapy. Recently, active surgical needles are getting attention due to their improved steerability and

capability for accurate placement in many medical applications. The technology of robotic and active needles has come into consideration because of its reasonable cost, safety, and efficiency in performing a precise needle insertion. The technology also aims to offer an enhanced penetration inside the tissue to reduce tissue trauma and to provide an enhanced needle tip visualization for tracking. The application of the active needles in percutaneous surgical procedures such as brachytherapy and biopsy are shown in this work.

Brachytherapy, a kind of radiation therapy, is considered as one of the most effective treatments for prostate and breast cancer that can be also used as a procedure for tumor treatment in other parts of the body. Brachytherapy is a compatible method that empowers doctors and surgeons to plant tiny radioactive materials, called seeds, inside the prostate to kill the cancerous cells in prostate cancer. Brachytherapy may also be used for breast cancer treatment, which usually happens after lumpectomy, to deliver small pieces of radioactive seeds in the area where cancer was initiated. Brachytherapy has applications for other types of cancer which are not relevant to the purpose of this study.

Biopsy is a sample cell or tissue extraction which is usually done by a surgeon, interventional radiologist, or an interventional cardiologist to specify the disease presence or extent. When an entire lump or suspicious area is removed, the procedure is called an excisional biopsy. Biopsies are a very common procedure that are studied and tested for better understanding and treatment of cancerous and inflammatory conditions. Performing several methods such as fine needle aspirate (FNA), core needle biopsy (CNB), or surgical removal, biopsy could be used for breast cancer diagnostic. As soon as a suspicious lesion is recognized, the operation of breast biopsy could be applied to take a partial of cancerous tissue out. These sorts of examinations may be visualized using ultrasound, magnetic resonance imaging (MRI), or stereotactic techniques that will be discussed in more detail through future sections. In addition, biopsies can be performed to assess prostate cancer by removing samples taken via an inserted hollow needle-core in prostate gland. As mentioned before, needle-based procedures investigation in cancer intervention and diagnosis is highlighted as the main purpose of this study.

Bevel-tipped hollow needles can also be used, inserted through human tissue, to reach the target diagnosed with cancerous or suspicious tissue. For this matter, precise needle tip placement at target position either for medical seeds delivery (in prostate brachytherapy) or tissue extraction (in breast biopsy) is very essential. Advantages of needle insertion procedures are listed as a more

successful operation due to higher reachability, less tissue rupture or damage, more valuable results because of accuracy, accessibility to various organs and body parts, and so on. In other words, the significance of needle-based procedures is not only maximizing the precision of surgeries in cancer treatments, but also minimizing the incision sizes and number of insertions to lessen the damage in patients' body. Such procedures will be discussed in the next sections to give a better understanding of their application and implantation.

1.2. Needle steering in tissue to reach accurate target

Needle-based methods are commonly used in minimally invasive clinical and surgical procedures to diagnose and treat cancer via different proceedings such as biopsy, drug delivery, and radioactive seed implantation. Conventional rigid-body needles offer a straight path with a start point at the entry location of the initial puncture towards the target. This is considered a disadvantage in needle insertions because of the limitations on the accessibility to the targets and the possibility of puncturing other sensitive organs inside the body. These punctures might have long-lasting with serious side effects. Other percutaneous procedures that involve needle insertion could be listed as vaccinations, blood/fluid sampling, regional anesthesia, tissue biopsy, abscess drainage, catheter insertion, cryogenic ablation, electrolytic ablation, brachytherapy, neurosurgery, deep brain stimulation, and minimally invasive surgeries. Needle insertion procedures may be applied at various depths based on the applications and types of needles. In breast or prostate biopsies, for example, the targets are usually located at a depth of 5 to 10 cm [5]. Furthermore, using stiff needles can lead to significant errors in needle tip placements that could occur due to needle displacement, tissue deformation, and complicated needle-tissue interaction. In cancer therapy, poor placement of needle tip can cause misdiagnosis or mistreatments. For instance, misplacement of radioactive seeds in prostate brachytherapy can provide over or under treatment dosage to the tissue. Breast biopsy is another example in which the inaccurate needle tip placement can cause faulty detection of cancer malignancy.

Hence, steering needles could increase the effectiveness of needle-based procedures in cancer cases. With enhanced maneuverability of steerable needles, previously inaccessible target locations could be reached without any extra damage or rupture in the tissues or other organs along the path to the target. Flexible needles are proposed to facilitate needle insertion in a curved path and to potentially decrease the targeting error. Several research groups have developed various methods to make flexible needles for steering in the tissue.

Through a specified curved path towards the target and a motion planning, the flexible needles can reach the target inside the tissue while avoiding puncturing sensitive organs (or obstacles) [6]. Needle motion planning in a deformable tissue is a difficult clinical task. Considering the tissue viscoelastic properties and target movement during a needle insertion task, the needle trajectory planning can be challenging. In addition, with optimum determination of insertion points and

steering strategies, the motion planning can be more effective in improving the placement of the needle tip at the target [7]. In order to solve motion planning problems, several algorithms are available. For example, a Jacobian needle manipulation with linear and angular velocities was introduced for the needle steering [8]. Such needle steerability concepts are defined by a relationship between the needle tip and needle body velocities which can be written in terms of extremely small changes in needle position. Based on the needle and tissue configuration at each moment, the Jacobian matrix could be formed. Another approach that is used for needle steering is potential field where a parabolic potential is located at the target [9]. The motion planning algorithm, developed based on the relationship between the needle base and the needle tip motion, computes the gradient total potential field at the needle tip and its repulsion torque to set and calculate the desired tip and base displacement of the needle. Uncertainty in needle motion planning is considered as another motion planning difficulty to steer the flexible needles [10]. The motion planner is executed and tracked under ultrasound (US) image guidance [11],[12] in order to enhance the probability of success (i.e., reaching the specified target). The advantage of such procedures is to directly receive all required data from the captured ultrasound images. This approach has formulated the motion planning problem as a Markov Decision Process (MDP) using infinite horizon Dynamic Programming (DP) [10],[13]. Infinite horizon DP is programmed with no finite time horizon and therefore, when a transition is happening in needle steering, the next action is computed with respect to the current position of the needle tip and it is not dependent on the past actions.

Rapid re-planning introduces an approach to automatically steer the flexible needles within the tissue to obtain accurate trajectory during insertion [14]. In this approach, the motion planner is re-executed during the needle insertion to perform closed-loop control, and the needle tip position is estimated using an electromagnetic tracker. The accuracy of this approach is successfully demonstrated with an average of error less than 3mm. This approach generates multiple plans and chooses the best for control execution in order to sense the needle tip position within the tissue.

Moreover, needle steering can be done under a real-time fluoroscopic guidance where a closed-loop control and steering is demonstrated with the error level below 0.5mm for 40mm trajectory length [15].

An asymmetry-based needle steering as a motion planning approach [16] may be used where two high-level actions are executed which provides a high probability of obstacle avoidance. This

method could find the shortest path to target and investigate if navigation through narrow passages is required. To accomplish this task, a motion planning procedure called as Stochastic Motion Roadmap (SMR) [17],[18] is proposed which requires polygonal outlines of the obstacles in the imaging plane, the start pose of the needle, and a target location in the plane. The uncertainty in the needle steering is formulated using MDP process that was mentioned before. This approach improves the effectiveness of needle-based insertion inside the tissue-mimicking environment with a negligible error in 2D and 3D spaces. This algorithm generates the roadmap for SMR and real time re-planning. It then checks if the bevel tip is flipped to either control the planner or compensate the torsion and finally investigates target reachability. Needle insertion in 2D could be implemented with planning algorithm to overcome tissue deformation and correct needle tip localization while it is guided to avoid predefined polygon obstacles [19].

For needle steering in 3D, a feedback control along with helical paths may be presented to correct perturbations with varying the helix radius [20]. In this method, needle deflection is collected by an imaging feedback system which improves the needle trajectory to get as close to the planned target as possible with controlling of the radius and heading of the helix.

Nonholonomic kinematics model of the needle-tissue interaction is an example of the closed-loop control for improving needle steerability and precise targeting in many percutaneous therapies and diagnostic methods [21].

Needle steering trajectory might also be intelligently sensed by some sensors positioned along the flexible needle. Fiber Bragg Grating (FBG) sensor [22] located on optical fiber is a reasonable choice for the purpose of needle steerability [23],[24]. This sensor obtains the strain data of the flexible needle to controls the needle maneuverability on the path towards the target. The target accuracy based on such model is about 1.3mm for the insertion length equal 110mm.

Generally, the above-mentioned recent studies have introduced methods to improve the needle steering based on the defined insertion trajectory and flexible needle design to enhance the target reachability and minimizing the measured error while avoiding obstacles. It is obvious that the needle design and needle tip tracking play an important role in the accurate needle insertion system. This thesis is organized to demonstrate an automated needle steering in both air and tissue-mimicking phantom using different proposed transformative needles and tracking the needle insertion path with an ultrasound device. It will be explained in more detail in the next chapters.

1.3. Passive and active needles - literature search

1.3.1. Passive needles

Passive needles have been studied for medical injections and percutaneous therapies for many years. All medical syringes with their rigid body, used for fluid injections, are in the passive needles' category. In terms of the concept of this work, passive needles are introduced as flexible bevel-tipped needles that could not modify their trajectory by any external actuations. In other words, the bending is realized by the reaction forces from the needle-tissue interactions. The use of passive needles in needle insertion procedures has been studied both experimentally and numerically [25]. The study has estimated the required force for the needle insertion that happens while the needle is inserted into a deformable tissue. There are different relevant forces applied to the needle for insertion within the tissue. Stiffness and damping forces as well as the insertion force are examples of these interacting forces.

The amount of insertion force depends on the tissue properties that change based on age, mass, gender, etc.; thereby dynamic estimation of force is needed while the needle is passing through different medium inside patient's body (e.g., skin, muscles, etc.). The other factors that influences the amount of force are the needle geometry, scale, tip shape and material [26]. The needle then is deflected to the direction of the actuation force with respect to needle tip asymmetry. In addition, tissue deformation needs to be identified to have an accurate control of automated needle insertion [27],[28].

Based on the needle insertion method and tissue and needle characterizations, the mechanical interaction between biological tissue and the needle itself might change. For many clinical and non-clinical applications, the order-of-magnitude of this force plays an important role and could be found with respect to the median of the maximum force. Moreover, the needle-tissue interaction for surgical simulators and their application in both invasive and non-invasive interactions are studied in the literature [29].

Actuation forces, in addition to the insertion force, can be used in active needles to improve the needle performance [30]. Many researches have simulated the needle insertion procedure either including needle-tissue interaction forces [21],[31]–[34] or without considering such forces [35]–[41].

1.3.2. Active needles

Another group of surgical needles called active needles has been proposed and studied in the recent decade. This type of active needles is more effective for percutaneous therapies and diagnostic due to their functionality where the insertion trajectory can be corrected as the needle is inserted. Feasibility studies have shown that actuation force applied to active needle's body bends the needle during insertion to improve needle steerability. Datla et al. [30],[42] presented an energy-based model of active bevel-tipped needles considering the actuation force for needle deflection measurement in soft tissue. Their design includes attached Shape Memory Alloys actuators to control the needle curvature inside tissue. Ryu et al. [43],[44] proposed an active needle design that improves needle deflection under actuation forces while overcoming needle-tissue interaction forces. The prototype was made from SMAs to take the advantages of biocompatibility and superelasticity properties. He also investigated an experimental evaluation of an optical actuation procedure comprised of a single-ended sensor to track the deflected needle [45].

This work aims to develop active surgical needles design and application for procedures such as brachytherapy and biopsy capable of successful navigation inside the tissue through a trajectory towards a planned target.

1.4. Shape memory alloys as smart actuators - background

Shape Memory Alloys (SMAs) [46]–[50] are a group of material used in various types of applications in different fields. The SMAs are known for their "Superelasticity" to recover a large deformation, caused by loading condition, via temperature changes. SMAs can also produce a high rate of actuation energy density, known as Shape Memory Effect (SME). These unique characterizations of SMAs make them suitable for different applications such as sensing, actuation, absorption, and vibration damping. Actuation of SMAs refers to their SME behavior, which could be shown as a hysteresis cyclic diagram to represent phase transformation between *Austenite* at high temperatures, and *Martensite* at low temperatures.

SMAs' characteristics and thermomechanical behavior such as SME, superelasticity, and biocompatibility in addition to corrosion resistance make SMAs suitable to be used in biomedical applications. Particularly, Nickel-Titanium (Ni-Ti) known as Nitinol [51] (made of two elements of Nickel at ~50% and Titanium at ~50%) is a part of SMAs family used in some less invasive medical devices [52]–[54]. Some of the most popular medical and biomedical applications of SMAs are orthopedic, cardiovascular, dental applications, and surgical and clinical instruments [55]–[58]. Due to the biocompatibility and corrosion resistant, Nitinol is used in many biomedical applications. Considering the superelasticity characteristics, Nitinol stents have been used in order to treat artery disease where blood flow to the heart muscle is decreased. The Nitinol stents expand to a suitable diameter with adequate force to open the vessel lumen and to restore blood flow.

Additionally, it is essential to carefully consider the strain behavior of Nitinol whereas unrecovered strain might be demonstrated under a determined stress and temperature level [59]. There are several constitutive models that are developed in order to study the SMA behavior as a function of strain, stress, and temperature. Tanaka [60], Liang and Rogers [61], and Brinson [62] are listed as three constitutive models of SMAs which are used to study the SMAs static performances.

In the constitutive model developed by Tanaka [60], a one-dimensional (1D) martensitic phase transformation is assumed. This model defines the strain, temperature, and martensite volume fraction as the state variables. The phase transformation kinetics is also described as a function of stress and temperature. This model demonstrates the stress-induced martensite phase transformation only. Liang and Rogers [61] proposed a model based on the rate form of the Tanaka constitutive model [63]. Even though Tanaka, and Liang and Rogers models explain the direct

phase transformations from martensite to austenite and the reverse transformation from austenite to martensite, they do not describe the detwinning process of martensite [63]. Brinson model [62] has resolved this issue by defining the total martensite volume fraction as a summation of two terms; the stress-induced, and the temperature-induced martensitic volume fractions.

Brinson model [62], which describes one-dimensional behavior of SMAs, is appropriate for this work, as the SMA wires are used for actuation purposes. Brinson constitutive model defines the state variables stress (σ), strain (ε), and temperature (T) in term of the martensite volume fraction (ξ) where the martensite volume fraction (ξ) is the sum of stress-induced (ξ_S) and temperature-induced components (ξ_T):

$$\xi = \xi_S + \xi_T \tag{1.1}$$

The original form of the constitutive equation is as follows [62]:

$$\sigma - \sigma_0 = E(\xi)\varepsilon - E(\xi_0)\varepsilon_0 + \Omega(\xi)\xi_S - \Omega(\xi_0)\xi_{S0} + \Theta(T - T_0) \tag{1.2}$$

where $\sigma_0, \varepsilon_0, \xi_0, T_0$ represent the initial state of the material. Θ and Ω are the thermoelastic coefficient and the phase transformation coefficient, respectively. The modulus of elasticity (E) is assumed as a linear function of the martensite volume fraction:

$$E(\xi) = E_A + \xi(E_M - E_A) \tag{1.3}$$

E and Ω are also linearly related as follows:

$$\Omega(\xi) = -\varepsilon_L E(\xi) \tag{1.4}$$

where, ε_L is the maximum recoverable strain.

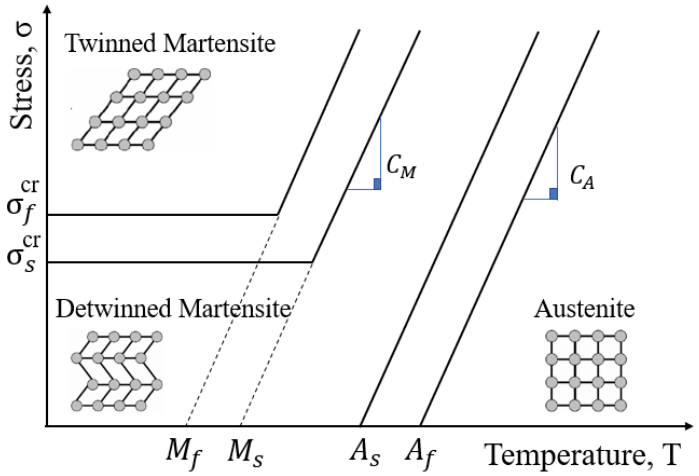

Figure 1. Critical stress-temperature profile based on Brinson Model.

Figure 1 indicates the linear relation between stress and temperature in Brinson model where σ_s^{cr} and σ_f^{cr} are critical start and finish stresses, respectively. Two material constants C_A and C_M

called as stress-influence coefficients could be experimentally determined, and they indicate the impact of stress on the transition transformation.

Considering Figure 1, the evolution kinetics equations to calculate the martensite fractions as a function of temperature and stress are defined as:

- Conversion to detwinned martensite

$$\text{For } T > M_S \;\&\; \sigma_S^{cr} + C_M(T - M_S) < \sigma < \sigma_f^{cr} + C_M(T - M_S)$$

$$\xi_S = \frac{1-\xi_{S0}}{2}\cos\left\{\frac{\pi}{\sigma_S^{cr}-\sigma_f^{cr}}\left[\sigma - \sigma_f^{cr} - C_M(T-M_S)\right]\right\} + \frac{1+\xi_{S0}}{2} \tag{1.5}$$

$$\xi_T = \xi_{T0} - \frac{\xi_{T0}}{1-\xi_{S0}}(\xi_S - \xi_{S0})$$

$$\text{For } T < M_S \;\&\; \sigma_S^{cr} < \sigma < \sigma_f^{cr}$$

$$\xi_S = \frac{1-\xi_{S0}}{2}\cos\left\{\frac{\pi}{\sigma_S^{cr}-\sigma_f^{cr}}\left[\sigma - \sigma_f^{cr}\right]\right\} + \frac{1+\xi_{S0}}{2}$$

$$\xi_T = \xi_{T0} - \frac{\xi_{T0}}{1-\xi_{S0}}(\xi_S - \xi_{S0}) + \Delta_{T\varepsilon} \tag{1.6}$$

$$\text{where, if } M_f < T < M_S \;\&\; T < T_0$$

$$\Delta_{T\varepsilon} = \frac{1-\xi_{T0}}{2}\{\cos[a_M(T-M_f)] + 1\}$$

$$else \;\; \Delta_{T\varepsilon} = 0$$

- Conversion to austenite

$$\text{For } T > A_S \;\&\; C_A(T - A_f) < \sigma < C_A(T - A_S)$$

$$\xi = \frac{\xi_{S0}}{2}\left\{\cos\left[a_A(T - A_S - \frac{\sigma}{C_A})\right] + 1\right\}$$

$$\xi_S = \xi_{S0} - \frac{\xi_{S0}}{\xi_0}(\xi_0 - \xi) \tag{1.7}$$

$$\xi_T = \xi_{T0} - \frac{\xi_{T0}}{\xi_0}(\xi_0 - \xi)$$

where a_A and a_M are material constants, in terms of transition temperatures A_S, A_f, M_S and M_f.

SMAs have shown to be an appropriate candidate for developing surgical needles and this paragraph provides some examples of that. Recent feasibility studies have specifically investigated the actuation capability of these alloys in different percutaneous procedures. Datla et al. [64]

developed an SMA actuated needle that demonstrates a control approach to navigate the needle through a curved path inside tissue. The SMA wires attached to the needle bend the needle when actuated. The work also considered the effect of SMA wires diameter in the amount of required current for actuation. Konh et al. [65] presented a feasibility study of SMA wire actuation for an active and steerable surgical cannula. Moreover, a 3D finite element prototype of such cannula was developed to investigate the active cannula's deflection upon actuation. The actuation capability of SMA wires and their complicated response to validate experimental tests have been considered. The active needle design was also optimized using an algorithm to increase proposed needle flexibility while inserting in tissue [66]. Moreover, Konh [67] modeled the solid-fluid interactions between the needle and tissue.

Joseph et al. [68] developed a position control system for robot-assisted SMA actuated needle in order to guide the needle through a curvilinear trajectory and reach the target. This self-actuated flexible needle is controlled by a robot to overcome the challenge of needle steering in percutaneous interventions. The simulation results of this work validate accuracy of curvilinear needle path trajectory to reach the defined target location. Furthermore, he and co-workers have introduced a closed loop nonlinear control of the SMA actuated steerable needle where the needle tip is controlled by electromagnetic, vision, and ultrasound imaging signals [69]. The results show that electromagnetic feedback signals have the most precise tracking efficiency among all.

In another work, Honarvar et al. [70] studied the strain response of SMA wires that could be modified based on any changes in other parameters such as stress level, wire diameter, and applied temperature. Generally, this work indicated strain behavior of the wires and their relationship with crystal structures of this material. He previously presented a nonlinear algorithm to control an SMA actuated manipulator for both open and closed loop motion simulations [71].

In this work, the needle's tube as well as the actuators (i.e., attached SMA wires) are made of SMAs with superelastic and shape memory effect, respectively. The flexibility offered by the superelastic SMAs makes the needles bendable in various directions, while the shape memory effect offers a reliable actuation to apply bending forces to the needles.

1.5. Image-guided needle insertion - background and significance

Integrated medical systems, leveraging from robotics and medical imaging, have impacted modern surgeries in recent years. Image-guided procedures have been used in surgical procedures with enhanced visualization of internal organs. In these procedures, the surgeons take advantage of traceable surgical instruments to perform the tasks with more precision. Several imaging devices such as medical video camera, ultrasonic, electromagnetic, computed tomography or medical x-rays imaging have been extensively used. Image-guided surgery is beneficial in surgeries such as brain tumor removal where it is hard to reach and do operation due to the size and location of the tumor. Such systems boost effectiveness of minimally invasive procedures where they allow surgeons to follow their instrument inside the patients' body to visualize hidden and critical structures. The image-guided surgical procedures include several stages from medical image collection, image segmentation and analyses to provide a 3D model, model registration to patient's position for visualization, and procedure execution [72].

The significance of visualization is apparent in medical procedures such as biopsy and brachytherapy. Using imaging systems in needle insertion procedures improves needle guidance and positioning.

Needle steering when equipped with medical visualization such as ultrasound imaging can assist in path tracking minimum deviation from the desired trajectory [12]. Glozman and Shoham [15] presented a robotic system to steer a flexible needle whose shape is detected via fluoroscopic images in real time. Fluoroscopic imaging helps to model the needle tip trajectory before insertion. Reed et al. [73] developed a system to steer flexible needle using a low-level image-guided approach (stereo camera, 3D ultrasound, bi-plane fluoroscopy) to find the path trajectory in order to reach the target within the tissue. Precise targeting could be evaluated with an ultrasound machine connected to a transducer equipped with optical tracking marker [74]. Hong et al. [75] proposed an instrument that works with an ultrasonic image segmentation technique to modify the needle path trajectory in real time. This method provides a safe and precise needle insertion with controlling and correcting (if needed) the needle deflection via image processing. Vrooijink et al. [76] presented a real-time 3D imaging system to track a flexible needle inside tissue using a two-dimensional ultrasound probe placed at the needle tip. While needle is inserted in tissue, transducer moves with the needle tip for visualization. The transducer movement is controlled automatically and performed using a compensator to check if the needle is out-of-plane and correct its insertion

velocity afterwards. He has also developed a novel needle steering system where the needle tip is tracked using a 3D online ultrasound-based method with a motion planner [77]. Furthermore, an automated needle segmentation algorithm that uses an orthogonal 2D image projection was presented by Ding et al. [78]. A technique based on 2D ultrasound imaging is proposed by Pourtaherian et al. [79] for a 3D Gabor transformation application. Using orthogonal projection increased needle insertion path tracking and thereby improved targeting accuracy. Abayazid and co-workers [80] presented a system which uses a three-dimensional ultrasound guidance to track needle steering inside a biological tissue while avoiding obstacles. The state-of-the-art ultrasound imaging system could detect a target as small as 2mm and update the needle path trajectory accordingly to reach the target. In addition, they investigated an image guiding approach to steer the needle in curved surface tissue where transducer is aligned with maximum contact area to obtain good quality images [81]. Ungi et al. [82] proposed an ultrasound guidance method where a transducer tracks the needle electromagnetically to enhance accuracy of targeting in facet joint injections. Tracked ultrasound snapshots (TUSS) were then recorded to help and improve guidance. Chatelain et al. [83] also presented a manual tracking method in real time with a 3D ultrasound transducer controlled by a robot arm. This system includes online image processing which is a combination of Kalman Filter and Random Sample Consensus (RANSAC) to track the needle and develop autonomous needle insertion procedure. Boctor et al. [84] developed acoustic ablator which is steered and tracked under a 3D ultrasound image guidance to facilitate needle monitoring inside liver tissue to place the needle tip at target.

Boctor et al. [85] also offered a three-dimensional ultrasound system reconstructed from 2D scans that helps needle repositioning to find the pre-planned trajectory for insertion. This image guiding system adapts a 3D visualization package to control the robotized system while minimizing the needle placement error. Image-guided percutaneous procedures track robotic needle insertion for precise positioning under computer control [86]. A 3D volumetric visualization could be performed using two-dimensional probe which is guided with an ultrasound system [87]. Doppler ultrasound imaging also visualizes the steerable needle with high frequency vibration [88]–[90]. Waine et al. [91] introduced a 2D ultrasound imaging for needle tracking which estimates needle tip deflection using a needle-tissue interaction model. Wong et al. [92] also investigated a new tracking system called SonixGPS [93] for needle insertion procedures and visualized needle tip to improve ultrasound-guided spinal anesthesia in real time. A literature

review of needle insertion procedure such as biopsy and brachytherapy under ultrasonic image-guided methods is presented by Shen et al. [94]. This review indicates the importance of precise needle navigation and target recognition in diagnosis and therapies [95]. Additionally, a tissue (e.g., prostate) could be reached under imaging guidance using a novel manipulator that is actuated remotely [96],[97]. Schneider et al. [98] designed a needle insertion system under transrectal ultrasound image guidance (TRUS) which is spatially coupled to the insertion device. Fenster et al. [99] investigated the application and significance of a mechanical three-dimensional scanning system to optimize the resolution of captured images in different clinical and interventional approaches.

In general, ultrasound imaging provides precise needle placement within tissue and improves targeting due to visualization. It also tracks the needle to path through a corrected trajectory to get as close to the target as possible. This work introduces a needle control system where the path trajectory of needle is traceable with a 2D transducer connected to a Doppler ultrasound machine.

1.6. How this thesis is arranged

The introduction part of this work describes the significance of needle-based procedures in cancer interventions, diagnosis and therapies such as biopsy and brachytherapy. Precise needle tip placement and steering the needle through a desired trajectory inside tissue while avoiding obstacles are discussed as well. To demonstrate the advantages of active needles versus passive needles, Shape Memory Alloys (SMAs) are introduced as a proper material for needle actuation. A literature review about needle imaging guidance to track the needle tip within tissue, and precise needle tip placement is also presented.

The contributions of this work rely on novel design of the active needles with 3D manipulation at the tip, robotic manipulation via stepper motors, and ultrasound tracking of the needle. Three novel designs of active needles have been introduced to improve steerability of the needle tip in three directions. The active needles are tested in air and tissue to evaluate the needle deflection. The needle insertion process is motorized and controlled to provide an improved navigation inside tissue. Precise needle placement inside a tissue-mimicking phantom is then investigated using ultrasound visualization methods. Chapters 2 and 3 present the methods and results, respectively.

1.7. The purpose of this study including new active needle design: 3D printed and slotted needles, steerable active biopsy needle, motorized needle insertion system, ultrasound tracking, testing in phantom

There has been a surge of interest in investigating active flexible needles in interventional procedures such as biopsy and brachytherapy in recent decades. The active needles are significantly advantageous in many minimally invasive procedures where reduced tissue damage and enhanced targeting allow physicians and surgeons to increase the efficiency of surgery. Precise needle placement at the target position has been very challenging and plays an important role to improve needle insertion effectiveness. The motivation for this thesis was to introduce an active needle that can steer in the tissue in multiple directions accurately. As mentioned in previous sections, enhance needle steerability is considered as the main purpose of this work. A complete system including needle design, tissue-mimicking preparation, motorized guidance and control of the needle in tissue, and needle visualization using ultrasound imaging to track needle deflection is provided. The experimental evaluations are comprehensively explained in future sections.

Firstly, three novel biocompatible designs are proposed based on the shape memory alloys characterizations and specifications. One of these needles is fabricated using 3D printing technology and a soft joint to enable deflection in all directions. The second active needle is made of Nitinol tube with multiple machined slits to facilitate bending. The last designed needle is applicable to biopsy procedures to extract suspicious tissue while the needle is deflected in the tissue.

To evaluate needle steerability in air and tissue, a motorized setup with stepper motors and stepper motor controllers is developed. This system provides needle control and navigation within tissue where the needle curvature is formed using a motorized manipulator. The needle is deflected when SMA wire actuators are mechanically pulled or electrically actuated.

In addition, a phantom is used as a tissue replacement in needle insertion methods. This phantom is formed using a combination of regular plastic and softener to be as soft as real tissue. An approach is presented for making a high quality and low-cost phantom for needle insertion tests.

The last part is arranged to discuss about needle visualization and tracking by ultrasound imaging techniques. An ultrasound machine attached with a transducer collects needle deflections in 3D and transfers captured frames to a computer for further analysis. Ultrasound imaging is

introduced as a safe and suitable method to track the needle inside tissue that leads to accurate needle tip placement at target position.

Chapter 2. METHODS

Needle insertion and precise navigation of flexible needles are challenging due to the limitations introduced by various factors such as lack of active control, tissue friction, tissue deformation, and target movement. This chapter introduces a novel surgical needle activated by Shape Memory Alloys (SMAs) actuators. Bending forces of the actuators are used to steer the needle inside the tissue for precise navigation and accurate placement of the needle at the target. In addition, a motorized system is designed and developed to insert and/or rotate the needle during the insertion process for enhanced maneuverability. Needle displacement within the tissue is tracked by an ultrasound machine to evaluate needle deviation from the desired trajectory.

2.1. **Active needle design and fabrication process**

Recent studies have shown that needle steerability and trajectory tracking can be potentially improved by using an active needle with proper control. Conventional surgical needles are rigid, biocompatible and corrosion resistant for use in the human body. The rigid structure of the needles restricts the needle insertion in a curved path, and thereby a limited maneuverability. Enhanced flexibility of the needles is desired for the needle to bend inside the tissue for improved navigation through more complex trajectories. For active control and manipulation during insertion, several research groups have proposed different designs of active needles [30],[42],[43],[100]–[103].

This work introduces three novel designs of active surgical needles for biopsy and brachytherapy procedures. The active needles are designed to provide improved steerability, while minimizing needle tip positioning errors resulted from needle displacement and/or tissue or target deformation. The needles are initially tested in air for performance assessments. Using the controllable angular deflection of the needles, the surgeons can compensate for tracking errors to get the needle on the planned path. In addition, the needles are manipulated by SMA wires. The SMA actuators can be activated via Joule heating (if needed) to bend the needle tip in three directions.

2.1.1. 3D steerable needle design and fabrication via additive manufacturing process

The 3D steerable needle was initially modeled in SOLIDWORKS. Figure 2 shows the design of the needle which includes multiple rigid parts and a soft joint. The parts (except the tip which is attached separately) contain three pairs of holes (120° apart, diameter of 0.20mm) to host the SMA actuator wires. With additive manufacturing, the parts were printed using a highly accurate 3D printing machine named OBJET 350 [104],[105] which is advantageous in order to minimizing printing time, being user friendly, and maximizing productivity and reliability. The 3D printer, used to fabricate the parts, was able to print parts with horizontal layer thickness as fine as 16 microns (0.0006in.), and build resolution of 600 x 600 x 1600 *dpi*.

The needle's rigid parts (4.19mm OD and 3.00mm ID) were fabricated with Digital ABS2 Plus in ivory and green material that is compatible with the printer.

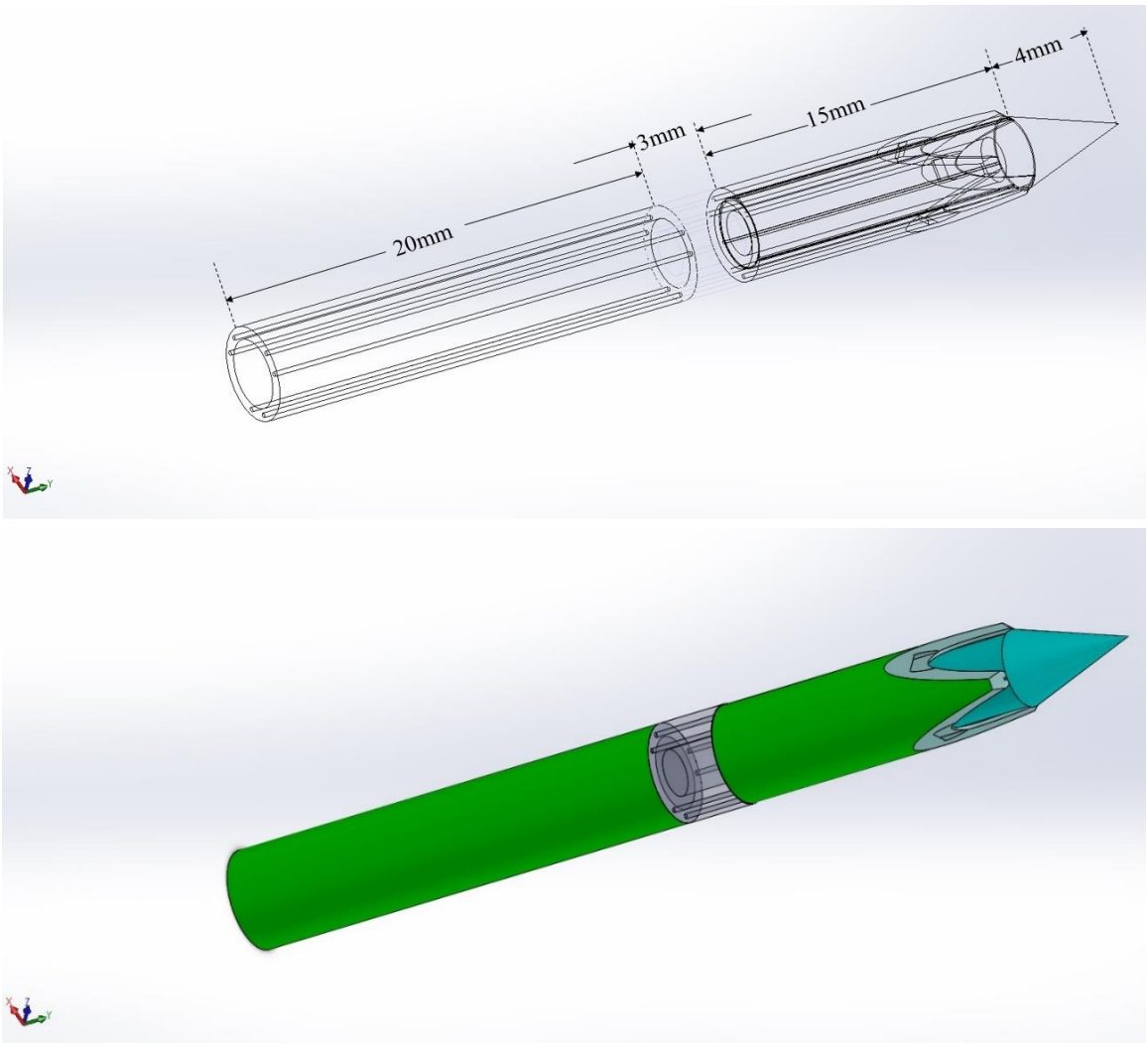

Figure 2. Schematic view of 3D steerable, 3D printed needle.

The parts were assembled, as shown in Figure 3, using three SMA wires passed through each pair of holes and looped at distal end. A sharp tip was attached to the tip to facilitate the initial incision in tissue. The SMA wires were actuated or pulled to realize bending at the needle tip. The flexible soft joint part was made of Digital Clear/Translucent Photopolymer material [104]. The 3D printed parts were attached to a Nitinol tube to make a longer needle for insertion tests.

Figure 3. Fabricated 3D steerable, 3D printed needle.

2.1.2. 3D steerable slotted needle and fabrication via machining process

Another innovative design which increases needle tip flexibility was also introduced and modeled in SOLIDWORKS. The schematic design with the dimensions is shown in Figure 4. For fabrication, a Nitinol tube (2.0mm OD and 1.6mm ID) was used as the needle's body. For 3D manipulation and improved flexibility, the Nitinol tube was slotted with a series of small slits (each 1.6mm long and 1.5mm wide). The slits were arranged evenly (120° apart) to enable bending in three directions. Three slits were made at the needle's distal point in Direction 1, followed by two slits and one slit in Directions 2 and 3, respectively.

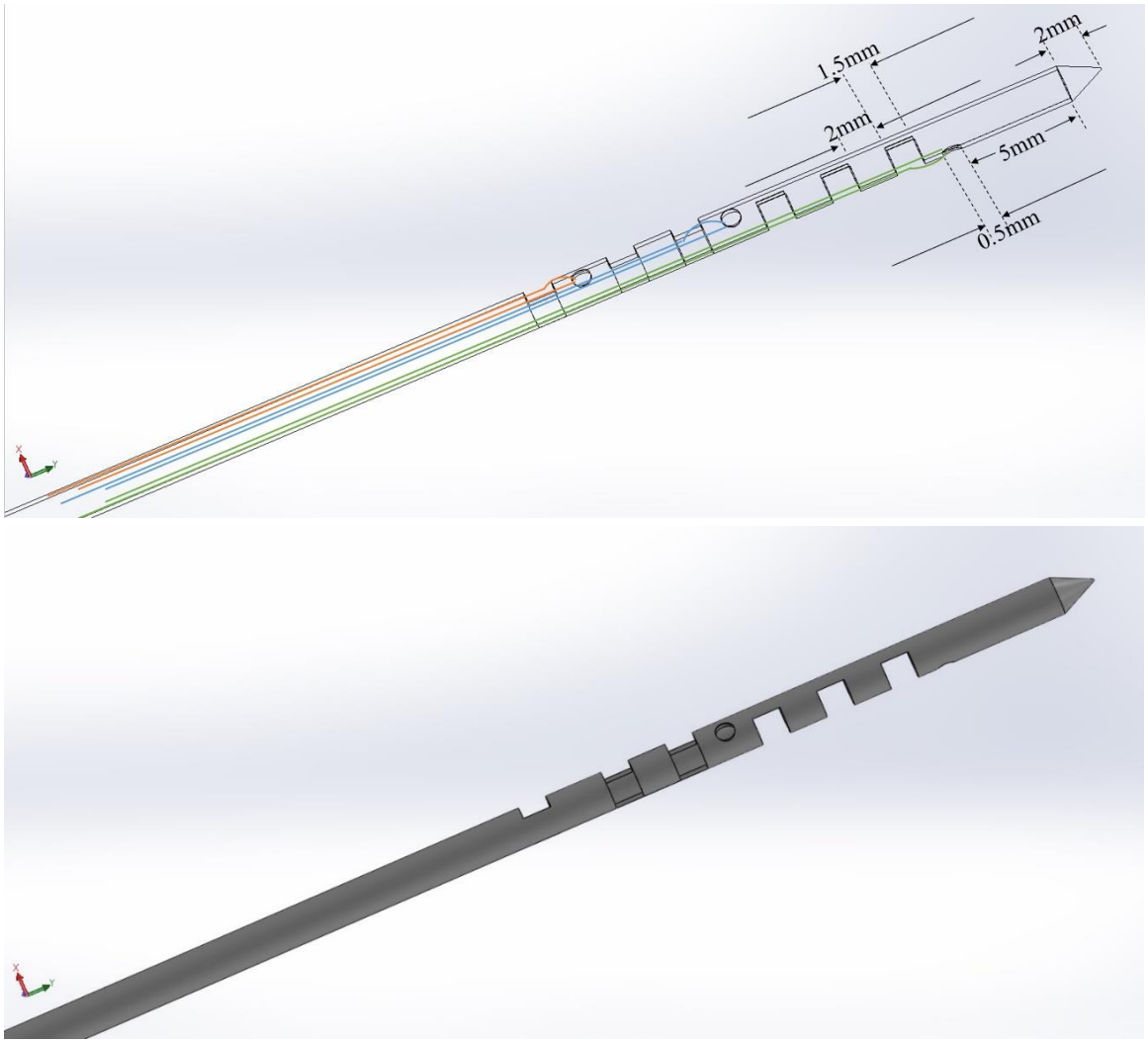

Figure 4. Schematic view of the 3D steerable slotted needle.

Cable tendons (i.e. SMA wires) were used to actuate the needle at its bending section in each direction. These wires could also be pulled to make a curved path for needle insertion within tissue. A sharp tip was attached to the tip to cut tissue as needle advances inside the tissue. Figure 5 shows the fabricated needle with the attached cable tendons.

Figure 5. 3D steerable slotted needle made with Nitinol tube via machining process.

2.1.3. Steerable active biopsy needle

The design of the flexible section of the biopsy needle is similar to the slotted needle. However, an extraction mechanism similar to conventional core biopsy needles is needed to take tissue samples. This needle is designed to investigate the tissue extraction when the needle is bent in one direction only.

A sharp bevel-tipped tray was made and passed inside the hollow needle to extract tissue. A wide cutoff (10mm long and 1mm wide) was formed on the tray. The axial movement of the tray inside the Nitinol tube was enabled using a plastic fixture attached to its end. Since the tray is supposed to be flexible to follow tube's curvature and bend in tissue, it is also fabricated with Nitinol material. The fabricated 1D steerable biopsy needle is shown in Figure 6a, with the extraction tray shown in Figure 6b. The main body of this needle is made of a Nitinol tube (2.0mm OD and 1.6mm ID). The Nitinol tube was slotted with three small slits (each 1.6mm long and 1.5mm wide) to enable bending in one direction. SMA wire actuators were attached to the needle to provide sufficient bending moment either by pulling or actuating the tendons.

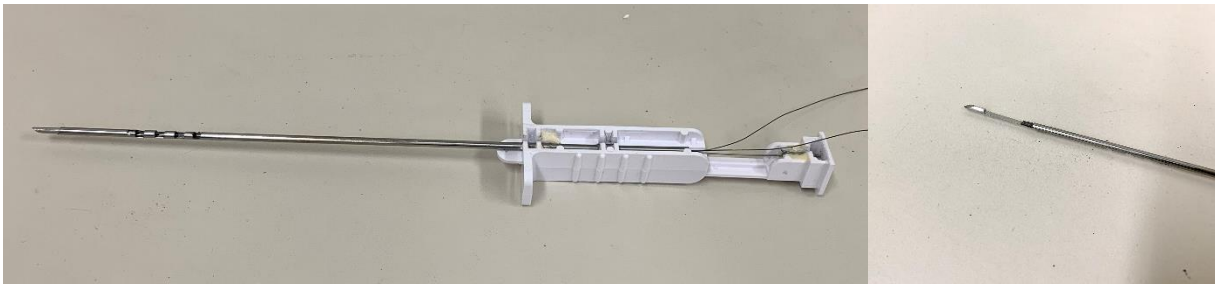

(a) (b)

Figure 6. Fabricated steerable active biopsy needle.

These proposed needles have been tested in air and in tissue to evaluate the angular deflection in three directions, which is the main purpose of this study. All obtained results are collected and explained in Chapter 3.

In comparison with the 3D steerable slotted needle (shown in Fig. 5), the steerable active biopsy needle (shown in Fig. 6) has only one set of slits in one direction to bend the needle and extract tissue samples.

2.2. **SMA wire insulation for electrical actuation**

Considering SMA actuation properties, the Nitinol needle can be bent upon SMA actuation. The actuation happens by Joule heating method and providing electrical power to the wires. The electrical power causes a temperature raise in the SMA wires, followed by a phase transformation which results in wire contractions, and needle bending. This phase transformation process is known as Shape Memory Effect (SME). Since the needles are made of Nitinol, and SMA wires are looped and passed inside of the hollow tube, the SMA wires should be insulated for proper actuation. Wire coaptation with chemicals, inner insulation of the needles, and wires coverage with tiny plastic tubes are among the options.

2.3. **Motorized needle insertion system**

Percutaneous needle-based procedures can be done manually or robotically. Needle insertion, as an example of percutaneous interventions, could be done manually that highly relies on the dexterity of needles and expertise of the operators. In manual needle insertions, the placement accuracy might be limited due to complexity of the operation where a visual feedback such as an imaging modality is used to track the needle. Even though manual needle insertion may seem to be beneficial as a basic study to improve percutaneous procedures, it has some disadvantages that could impress the insertion in many aspects. The main disadvantage is an increased tissue damage or rupture that occurs due to needle displacement or surgeon hand's tremor.

Hence, robot-assisted procedures are used to overcome these limitations and enhance the accuracy of needle placement in most of minimally invasive surgeries [106]. In robot-assisted procedures, the accuracy of the needle insertion and placement strongly depends on precise robotic motion, tissue deformation, and accurate prediction of needle deflection with respect to the needle tip position. In robotic insertions, the needle is inserted and steered in soft tissue via a robotic manipulation [107].

This chapter presents an automatic needle insertion method in soft tissue. The axial movement is realized by a programmable stepper motor to guide the needle inside the tissue. Stepper motors are brushless DC electric motors where the motor rotation is divided into several equal steps. When the motor is properly commanded in respect to torque and speed, the motor's position can be controlled to move at these steps. These motors could receive an electrical power and convert it into a mechanical rotation. There are two windings arrangement named Unipolar and Bipolar for electromagnetic coils in a two phases stepper motor. Unipolar stepper motor has one winding with center tap per phase, but bipolar stepper motor has a single winding per phase. Stepper motors usually come with four, five, or six wires where a four-wire stepper motor is used with a bipolar driver only. Stepper motors are attached to a driver (e.g., a microcontroller, stepper motor controller, or other motor drivers) and motor performance is extremely dependent on it. Stepper motor controller is a device that includes motor driver and governs the performance of stepper motor. The controllers could work automatically with a half-step switching sequence to drive the motors. It also increases the motor torque and optimizes the motor efficiency that leads to higher resolution and better performance.

To perform a needle insertion task in this work, as shown in Figure 7, a motorized system is set up including stepper motors, stepper motor controllers, XSlide positioning stages, motorized rotating table, motor dampers, power supply, cables, and aluminum profile. Two single shaft 2-phase stepper motors used in this system are called VEXTRA PK245-01AA [108]. According to the motor specifications, the motor shaft rotates 1.8° per step. Therefore, 200 steps are needed for motor shaft to rotate one full revolution:

$$steps = \frac{360°}{angular\ rotation\ per\ step} = \frac{360°}{1.8°} = 200$$

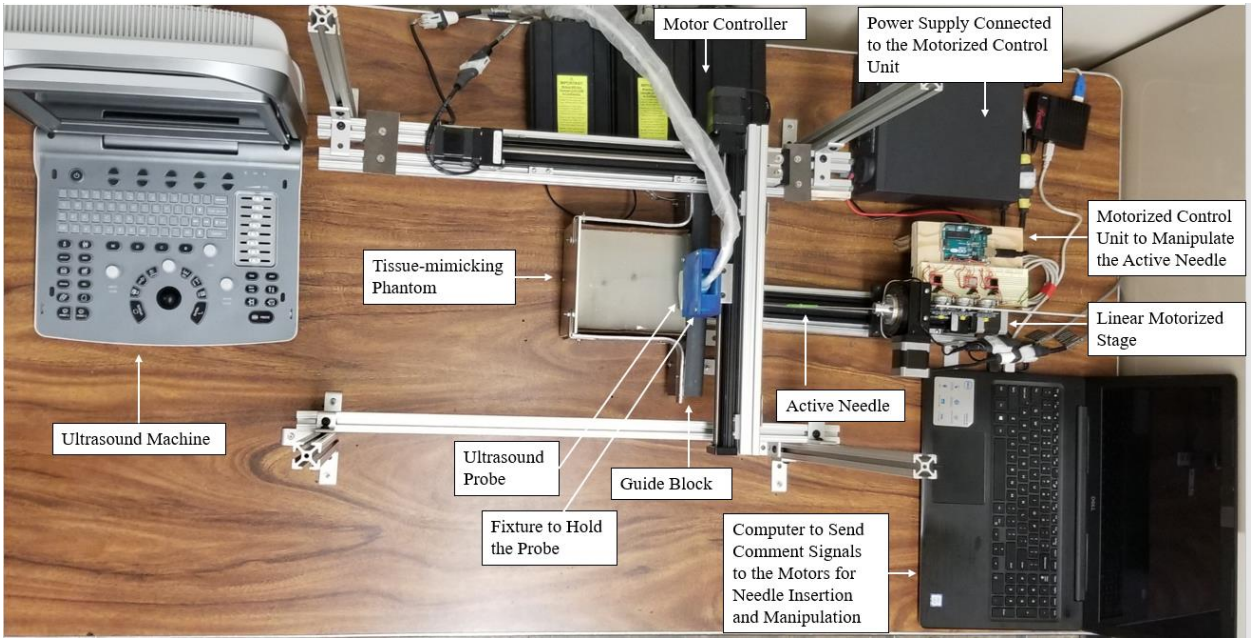

Figure 7. motorized needle insertion setup.

The needle insertion system is mounted on a table with aluminum profile supporting frames. The motors are connected to dampers and controllers to move the needle towards the tissue. The other rotary motor is attached and controlled to rotate the needle upon demand. The needle is completely fixed on the motors to prevent needle from sliding in the motors. Two other motors are attached to move an ultrasound probe on top of the tissue for scanning the needle tip (discussed later). The motors are programmed using MATLAB. Stepper motor controllers are connected to a computer via USB cables.

To manipulate the needle in multiple directions, a motorized system including three stepper motors are designed and assembled for pulling the wires to actuate the needle. Each stepper motor provides a step angle resolution of 7.5 degrees with 48 steps per revolution [109], which was

appropriate for this study. The assembled motorized system to manipulate the needle inside the tissue is shown in 9.

Figure 8 demonstrates the operational block diagram for the needle insertion inside tissue. The needle insertion system includes ultrasound probe, wire pulling, and insertion mechanisms operated by a MATLAB programmed interface.

Considering stepper motor specifications, the distance that needle travels from initial puncture towards the target should be calculated. The number of steps and motor shaft revolutions needed for a complete needle insertion in tissue should be coded in MATLAB. Based on motors' specifications and manual measurements, axial displacement of the motor can be found as the motor moves ($d = 7.5 \times 10^{-3}$ ($^{mm}/_{step}$)):

$$s \triangleq One\ full\ rotation\ of\ motor\ shaft = 200\ steps$$
$$d = 200 \times 7.5 \times 10^{-3} = 1.5\ mm$$

Hence, the motor moves the needle 1.5mm per shaft rotation in axial directions. Assembled compact positioning stage is 300mm long, where the motor moves from initial position to the end point. Because the needle is partially inserted in the tissue prior to actuations, motor could move forward for 270mm first (position 2), and it will be inserted more (with respect to the defined algorithm) after pulling wires. Therefore,

$$s = \frac{270\ (mm)}{7.5\times10^{-3}\ (^{mm}/_{steps})} = 36000$$

So, the motor moves 36,000 steps forward, then wires are straightly pulled to guide the needle tip to each direction and the motor moves for additional 9500 steps afterwards to complete the needle tip curvature and reach the target (position 3, position 4, or position 5):

$$d = 9500 \times 7.5 \times 10^{-3}\ mm = 71.25\ mm$$

The needle moves $341.25\ mm\ (= 270 + 71.25)$ from initial point in axial direction. This distance is modified for different needles with different length. Partial needle insertion inside tissue (position 2) helps to ensure the needle deflection in multiple directions. The probe also moves 110 mm forward or backward to track the needle from the edge of tissue to the target position.

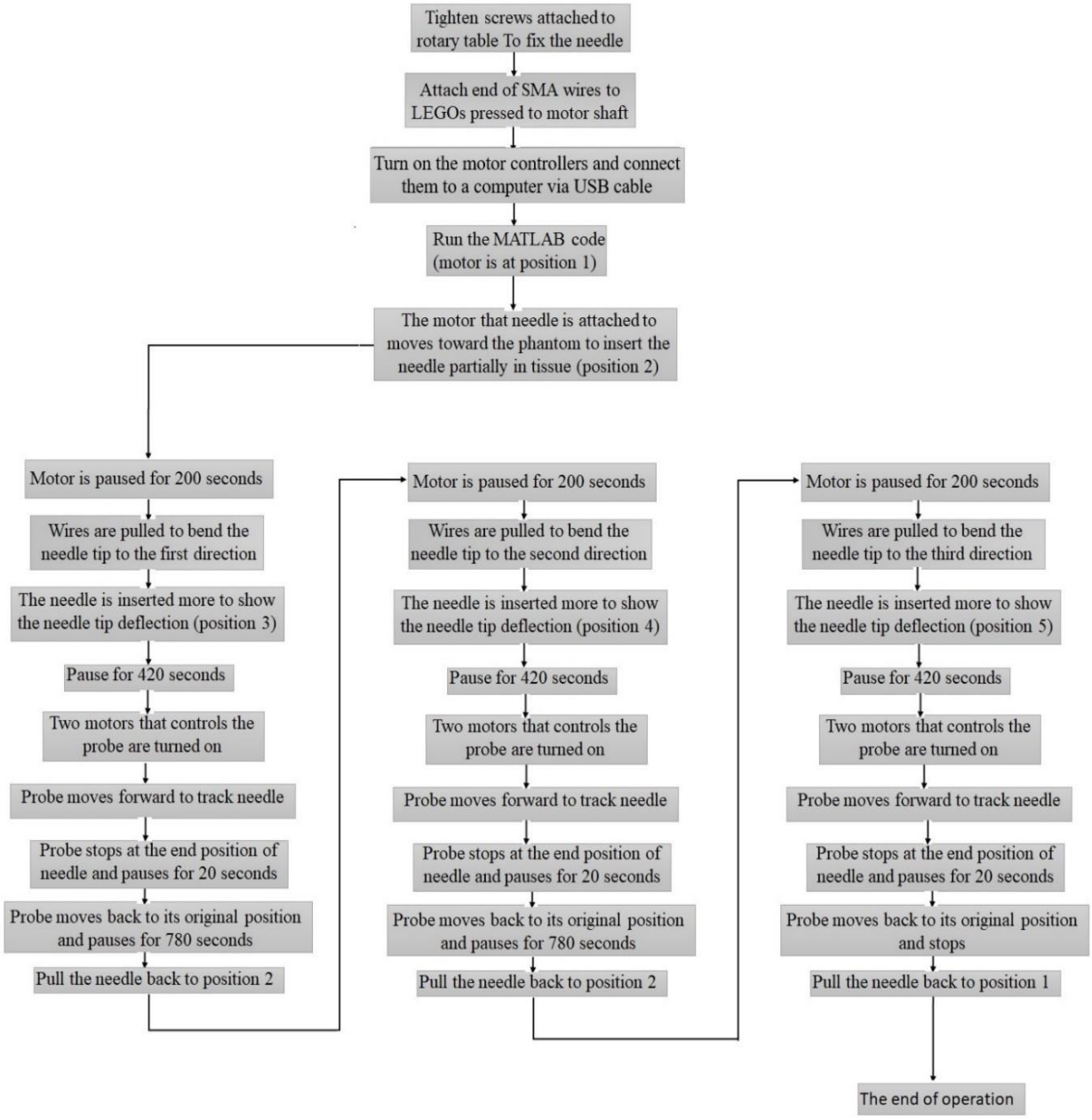

Figure 8. Needle insertion algorithm.

2.4. **Motorized manipulation for needle deflection**

This section presents a motorized system to bend the needle tip in multiple directions. The system is applicable to any needle design that includes tendon cables (SMA wires in our design). Such cables are attached to the needle and might be actuated mechanically or electrically to make a desired curvature on the needle. Other research groups have investigated 3D steering of active needles when SMA wires are electrically actuated [110]–[112]. Needle tip deflection based on mechanical actuation of the wires is explained in this section.

To manipulate the needle in air or tissue, a cable-driven system is introduced and assembled. Three bipolar M25SP-5N stepper motors [113] were used to pull the cable tendons (SMA wires) to deflect the needle in three directions. The motors were attached to a circuit board and a motor driver. The motor driver converts a low-current signal into a high-current signal (sufficient power) to run the motors. An Arduino UNO was programmed to send command (electrical signals) through the circuit to rotate the motor shafts and pull wires to navigate needle tip to each direction. The tendon cables were completely fixed on pulleys, which were then tightly pressed on the motor shafts (as shown in Fig. 9). It should be noted that all cable tendons were completely stretched, prior to their attachment for calibrations, in order to keep the initial shape of the needle straight for the initial puncture. Predefined values in Arduino code for stepper motor speed and number of revolutions are 60 *rpm* and 1 (i.e. 360°), respectively. The application of this system for needle steering in air and inside tissue is explained in Chapter 3.

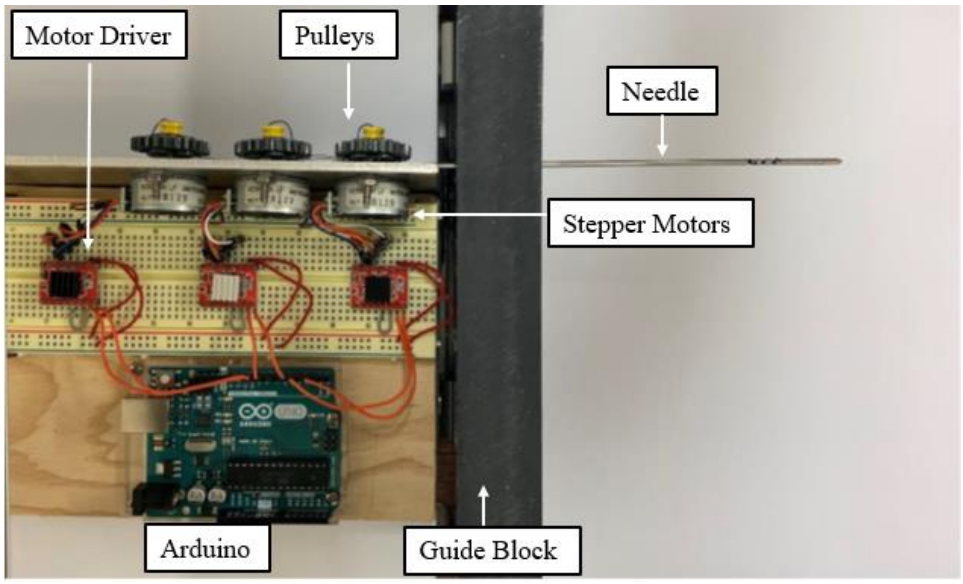

Figure 9. Motorized system to manipulate the needle in air and inside tissue.

2.5. **Ultrasound tracking: setup and image transfer**

Ultrasound (US) systems have been used since the 1950s [114]. Their application in medical diagnosis has made them well accepted in diverse medical fields. Ultrasound machines have been widely used in educational systems for researches as well as in clinical and medical systems.

To track the needle inside tissue, ultrasound machines are commonly used [115]. Ultrasound machines provide an internal image of the tissue (i.e., tumor) and the needle for the surgeon to visualize during a needle insertion process. There are some factors which should be manually set on the US machine to get a high-resolution image, which is suitable for tracking the needle in real-time without missing the needle tip in any frame. This section suggests an effective method to track the needle tip using an ultrasound machine with high-resolution images during the needle insertion.

The US machine used for this work was Digital Color Doppler Ultrasound CHILSON ECO 5[116]. This machine has the capability to tune several parameters depending on a specific tissue. Table 1 shows changes that were applied in the parameters of captured images by the US machine to record the best images during the needle insertion.

Table 1. Setting parameters on the ultrasound machine.

Parameter / Mode	FPS	GN	PWR	FRQ	DN	D
B Mode	79	90	15	10M	74	3.7cm

A brief description of factors (mentioned in Table 1) to be tuned before using the ultrasound for tracking is presented:

B-Mode: A key is placed on ultrasound machine to tune the system for the display mode which is known as the brightness mode. It is a basic mode to diagnose and scan an area of the human body visualized as a 2-Dimensional image on the screen [116],[117].

FPS: Frames per Second indicates frame rate in the frequency rate. The ultrasound system was able to generate images at a rate of hundreds of FPS using high range of frequency [116]**.** The range of 60 to 90 is reasonable for the matter of this paper and 79 gives the best result.

GN: It represents Gain in an image which shows how dark or bright the recorded images are. Otherwise stated, it shows the speed rate of waves sent in real time. The ultrasound system has a

range of 0-255 (with step 5) for gain [116]. Tuning gain plays a key role in increasing the resolution of each captured frame. The value 90 is fair enough for this test.

PWR: It points to PW Doppler where the velocity of moving tissues and fluids matters during data measurement. It could be combined with B-mode for examinations [116].

FRQ: This factor represents Frequency of the collected images from testing. The Ultrasound machine operates with a wide-spreading range of frequencies [116]. It is usually considered aorud10MHz.

DN: Stands for Dynamic in B-mode for the contrast resolution adjustment which has a range of 30-90. It is optimal for the DN value to be around mid of this range (i.e. 50-70). This is one of the most important parameters to specify the image quality where measuring the difference between maximum and minimum displayed values of a signal is considered [116],[118].

D: Stands for Depth of influence that is linked to waves frequency where shorter depth is related to a higher frequency. Therefore, for clinical purposes, it is better to tune the system to a lower frequency in order to have a greater depth [116].

STC: Additionally, there are eight slides on ultrasound machine that are used for penetration gain adjustment in different image depths. Tuning these slides is necessary to make the image lighter or darker. The default on one-half or one-third will capture higher quality images [116].

With all US settings properly tuned, the position of inserted needle in phantom was tracked. The needle tracking was accomplished via a Python code through an automated process of displaying the images and storing them on a computer as a video file as well as capturing and saving each frame separately.

2.6. **Phantom preparation**

2.6.1. A brief background of tissue-mimicking phantom

For preliminary needle insertion tests, it is mostly desired to use phantom material instead of real tissue for reasons such as cost, availability, and safety. These phantoms are not only useful for estimating the needle behavior inside the tissue, but also can be used to train novice surgeons in needle insertion tasks [119],[120]. In many cases, several needle insertion tests are required before achieving a reasonable estimation for a new needle insertion method; therefore, several phantoms might be used for a single study; this can be very costly. In biomechanical research, phantoms are usually made according to standard testing protocols [119] to mimic the properties of the tissue [120]. One important task in phantom preparation is to alter its stiffness [120] to match the stiffness of a desired tissue. The stiffness of many tissues can be found in available literature [121],[122].

2.6.2. Soft tissue phantom preparation

Materials such as gelatin powder, Polydimethylsiloxane (PDMS) [120], or modified composite hydrogels [119] have been commonly used to prepare phantom materials. In this work, phantoms were made using liquid plastic base [123], with a portion of plastic softener to tune the phantom's stiffness. Depending on the modulus of elasticity of the tissue, plastic hardener was also added. In order to experimentally evaluate the needle tip tracking, four phantoms were prepared, each with a different proportion of plastic softener and stirring period, which led to different levels of transparency.

Firstly, liquid plastic and an appropriate amount of softener (Fig. 10) were poured into a small aluminum pan and heated slowly up to 350ºF until the liquid thickened and turned clear. Right after, stirring was initiated until a pouring quality was attained and the color changed into a transparent white. One important observation was that rapid stirring helped the liquid to be unified but also generated a lot of bubbles, which affected visualization. The product was then poured into a square container and kept at room temperature for 24 hours until fully solidified prior to use in needle insertion tests.

A transparent and bubble-free phantom [124] made for the purpose of this thesis is shown in Figure 11. To prepare this phantom, a vacuum oven was heated up to 220°C (428°F) to bring up all bubbles to the surface of liquid. The top layer of liquid was then removed in order to procure a phantom free of bubbles. The ration of regular liquid plastic and plastic softener plastic to prepare

this phantom is 1:2 (i.e. 1000 ml regular plastic and 500 ml softener). Moreover, the required stirring time to end up with a very clear phantom is 90 minutes approximately. The stirring time is different based on the volume of liquid.

Figure 10. Regular liquid plastic (right) and plastic softener (left).

Figure 11. Soft tissue-mimicking phantom.

As demonstrated in Figure 12, a phantom with an embedded male pelvic skeleton and prostate phantom is also prepared for brachytherapy needle insertion. The regular liquid plastic and the

softener plastic ration to make this phantom is 3:2 (i.e. 2400 ml regular plastic and 1600 ml softener).

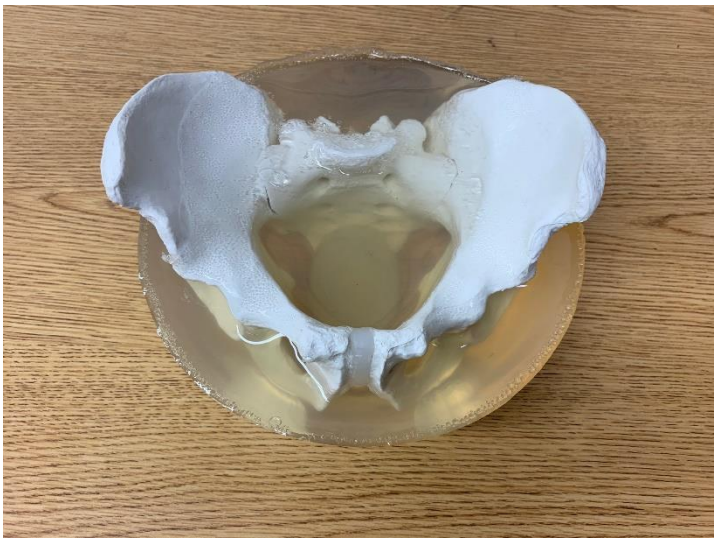

Figure 12. Prepared phantom with an embedded pelvic skeleton and prostate.

For needle insertion tests, these phantoms could be a substitute for real tissue. The main advantage of using the liquid plastic to prepare the training phantom was its affordable price. This experiment demonstrated the potential of developing a high-quality custom-made phantom, which can be molded into any desired shape. Both vision-based techniques (e.g., using cameras), or the ultrasound tracking can be used to track the needle inside the phantoms.

Chapter 3. **RESULTS**

This chapter demonstrates the experimental observations and measurements using proposed needles to evaluate their effectiveness for needle-based procedures. The results show that the desired amount of needle deflection in air and tissue-mimicking phantom is achieved.

3.1. Needle deflection in air

This section explains the needle deflection measurement and evaluation in air. The three proposed needles were tested in air first to measure needle tip bending without tissue resistance. Needle deviates as soon as tendon cables (SMA wires attached to the needle) are pulled or actuated. The needle tip deflections in different directions (schematically shown in Fig. 13) are discussed below. The following sections summarize the results.

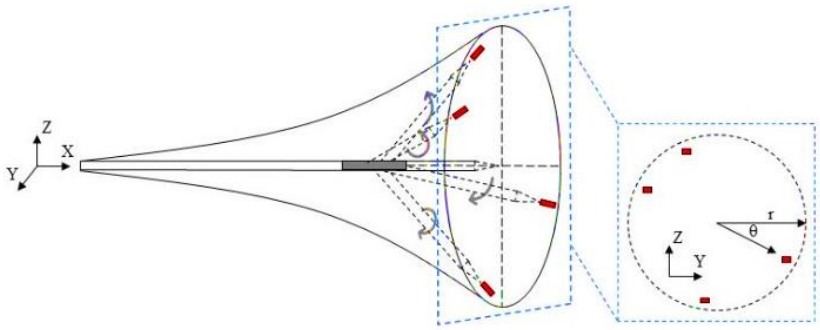

Figure 13. Accessing various part of tissue via the 3D steerable active needle.

3.1.1. Needle actuation in air

The experimental setup (shown in Fig.14) was developed to assess the needle deflection in air. The needle was kept vertical at its distal point, and the end of the needle was fixed to an aluminum plate. All tendons were completely stretched by attaching small weights of 20 grams. For deflection, additional weights were added to pull the wires and force the needle tip to bend into the desired direction. To collect result, a camera was located above the needle to capture a video from the needle tip deflection in three directions. The videos were then processed in MATLAB to track the needle tip using a video tracker code [111].

Needle deflection in three directions was measured for the three proposed needles. The amount of force applied to the tendons by attaching extra weights was chosen based on needle fabrication and the SMA wires diameter.

Figure 14. Test bed setup for in air experiment.

3.1.1.1. Deflection of the 3D steerable, 3D printed needle in air

The needle, presented in Chapter 2, includes two 3D printed parts and one soft joint placed in the middle. The dimension of SMA wires attached to the needle was 0.005in (0.127mm). Each wire is under pre-pressure by attaching 20 grams to ensure all wires are straight. So, the amount of stress on each wire (by attaching weight equals 400 grams) can be estimated as:

$$A = \frac{\pi D^2}{4} \tag{3.1}$$

$$A = \frac{\pi \times (0.127)^2}{4} = 0.0127\ (mm^2)$$

$$\sigma = \frac{F}{A} = \frac{mg}{A} \tag{3.2}$$

$$\sigma = \frac{0.4 \times 9.8}{0.0127} \cong 309 \left(N/_{mm^2}\right) \cong 309\ (MPa)$$

where *A* is the cross-sectional area of the wire, *D* is the wire dimension, *m* is the attached weight, and σ is the stress applied to the wire. The needle deflection in three directions were realized as typically shown in Figure 15:

Direction 1 Direction 2 Direction 3

Figure 15. 3D steerable, 3D printed needle deflection in air (vertical view).

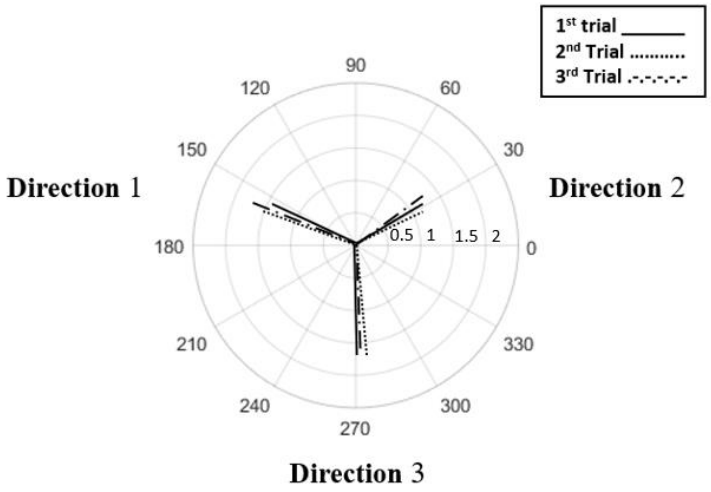

Figure 16. Shape of 3D steerable, 3D printed needle in air (vertical view).

3.1.1.2. Deflection of 3D steerable slotted needle in air

A higher pulling force was needed to deflect the slotted needle. The Nitinol tube showed a higher resistance to bending due to its superelasticity. To apply sufficient bending force to the needle tip, SMA wires of 0.01in (0.25mm) diameter were used. The amount of stress was calculated by attaching weights equals to 1520 grams. The deflections are typically shown in Figure 17 (all wires are straightened by attaching 60 grams to each of them):

$$A = \frac{\pi \times (0.25)^2}{4} = 0.049\ (mm^2)$$

$$\sigma = \frac{1.52 \times 9.8}{0.049} = 304\ \left({}^{N}/_{mm^2}\right) = 304\ (MPa)$$

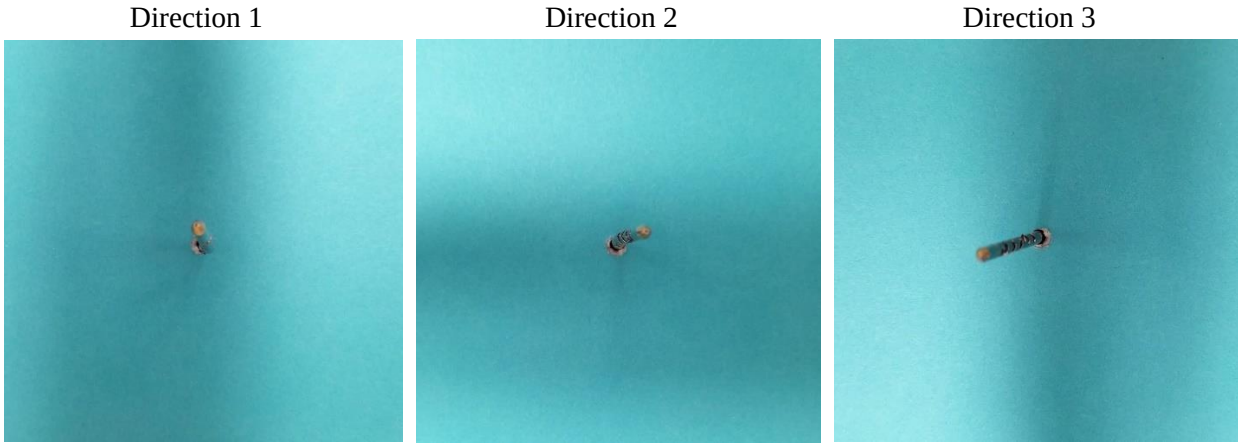

Figure 17. 3D steerable slotted needle deflection in air (vertical view).

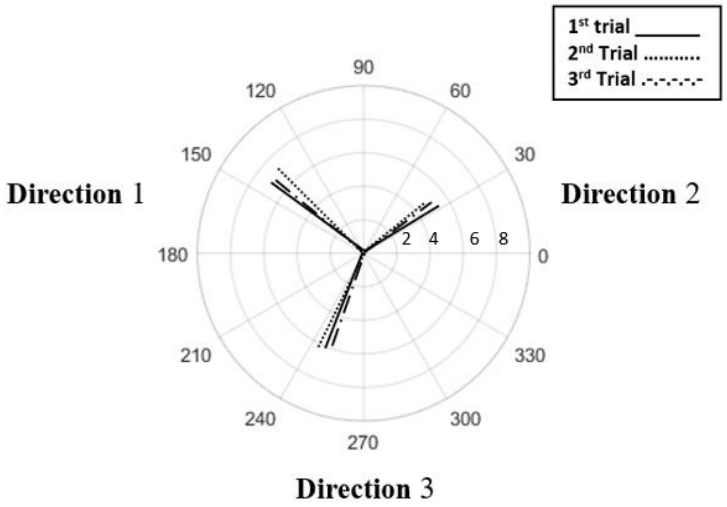

Figure 18. Shape of 3D steerable slotted needle in air (vertical view).

3.1.1.3. Deflection of the steerable active biopsy needle in air

To deflect the slotted biopsy needle (presented in Chapter 2), the SMA wires with diameter of 0.25mm under 304MPa of stress were used. The deflection of the slotted active biopsy needle is shown in Figure 19.

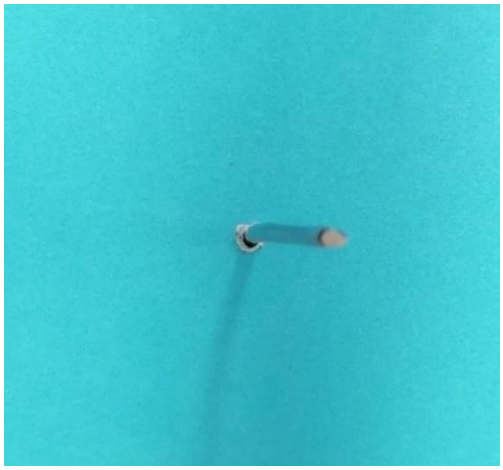

Figure 19. Steerable active biopsy needle deflection in air (vertical view).

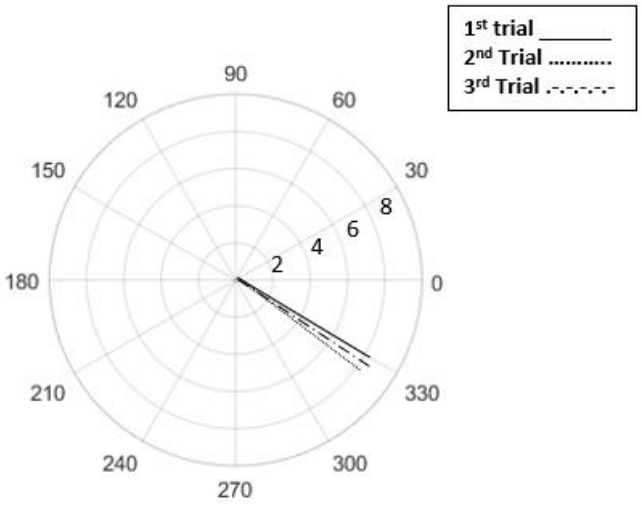

Figure 20. Shape of steerable active biopsy needle in air (vertical view).

Table 2 shows a comparison among three tested needles in three directions. Angular needle deflection in three directions of 3D printed steerable needle is more than steerable slotted needle due to the needle fabrication. Moreover, angular deflection of biopsy needle in one direction has the highest value.

Table 2. Averaged needle deflection measurement in air for three needles (vertical view).

Angular Deflection (degree)	3D Printed Needle	Slotted Needle	Active Biopsy Needle
Direction 1	11.80±0.12 (deg.)	11.50±0.28 (deg.)	14.15±0.34 (deg.)
Direction2	11.77±0.08 (deg.)	10.30±0.39 (deg.)	N/A
Direction3	12.10±0.09 (deg.)	11.05±0.11 (deg.)	N/A
Average	11.89 (deg.)	10.95 (deg.)	14.15 (deg.)

3.1.2. Motorized needle deflection in air

To measure the needle tip deflection in air, the setup shown in Figure 21 was used. Tendons were fixed on the pulleys which were tightly pressed on the motor shafts. The tendons were completely stretched. This section shows the needle curvature in air when the tendons are pulled by the stepper motors. The three needles were tested separately with this setup. The needle deflection was captured by two cameras from two angles (top and side views) to measure the amount of bending in three directions.

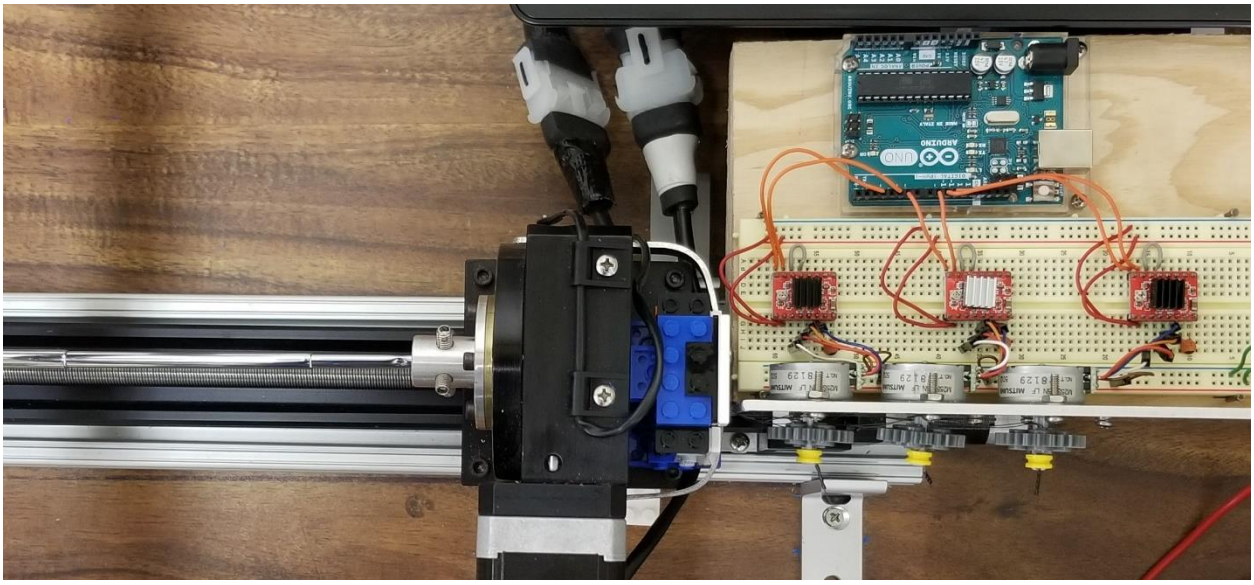

Figure 21. Setup for in air experiment included wire pulling system.

Considering motor specifications, the stepper motor needs a voltage in range of 21.6 ~ 26.4V to work. Therefore, a power supply was needed to generate enough voltage to rotate the motor

shaft and consequently pull the cables. Considering that the motor shaft diameter is 2mm, the generated force by the motors could be calculated as:

$$\tau \triangleq Holding\ torque\ for\ stepper\ motor = 18.9\ mN.m$$

$$\tau = F \times r \tag{3.3}$$

$$\xrightarrow{Force\ calculation} F = \frac{\tau}{r} = \frac{18.9}{1} = 18.9\ N$$

where r is the motor shaft radius. Hence, the motor could generate 18.9 N force, which supplies sufficient force for bending the needle in three directions.

3.1.2.1. Cable-driven deflection of 3D steerable, 3D printed needle

As discussed before, this needle includes a soft joint at bending (flexible) section, two rigid plastic part, and three cables passed through holes (three pair of holes 120° apart) that are printed on all parts. Needle curvature in each direction is realized by motorized wire pulling with the system introduced in Section 2.4. Figure 22 shows the deflection result with two cameras in three directions.

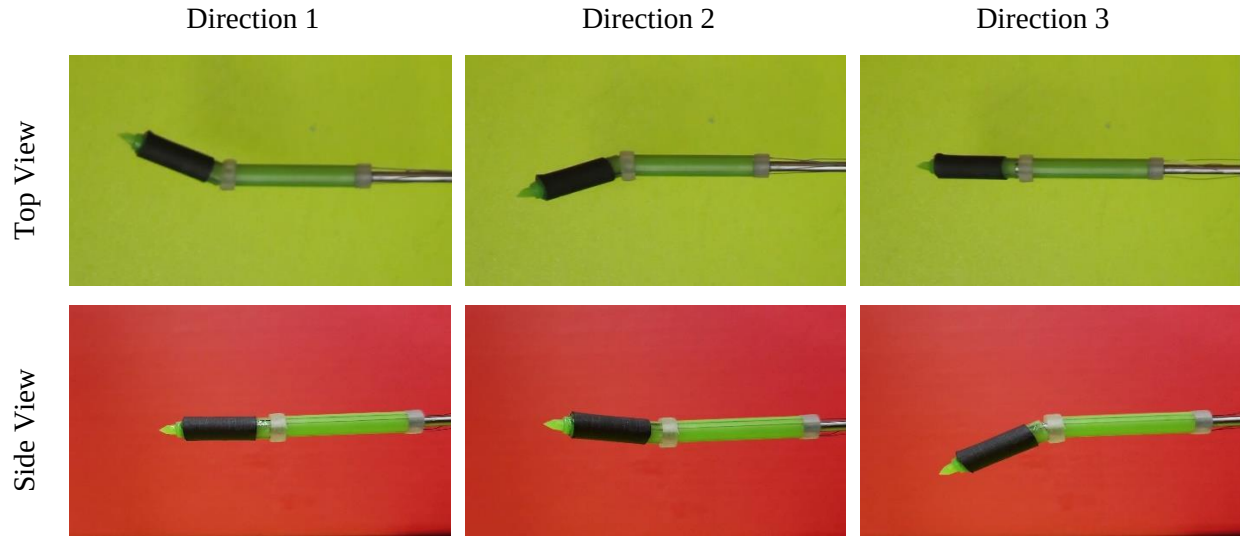

Figure 22. Top and side views of the 3D steerable, 3D printed needle deflection in air (horizontal view).

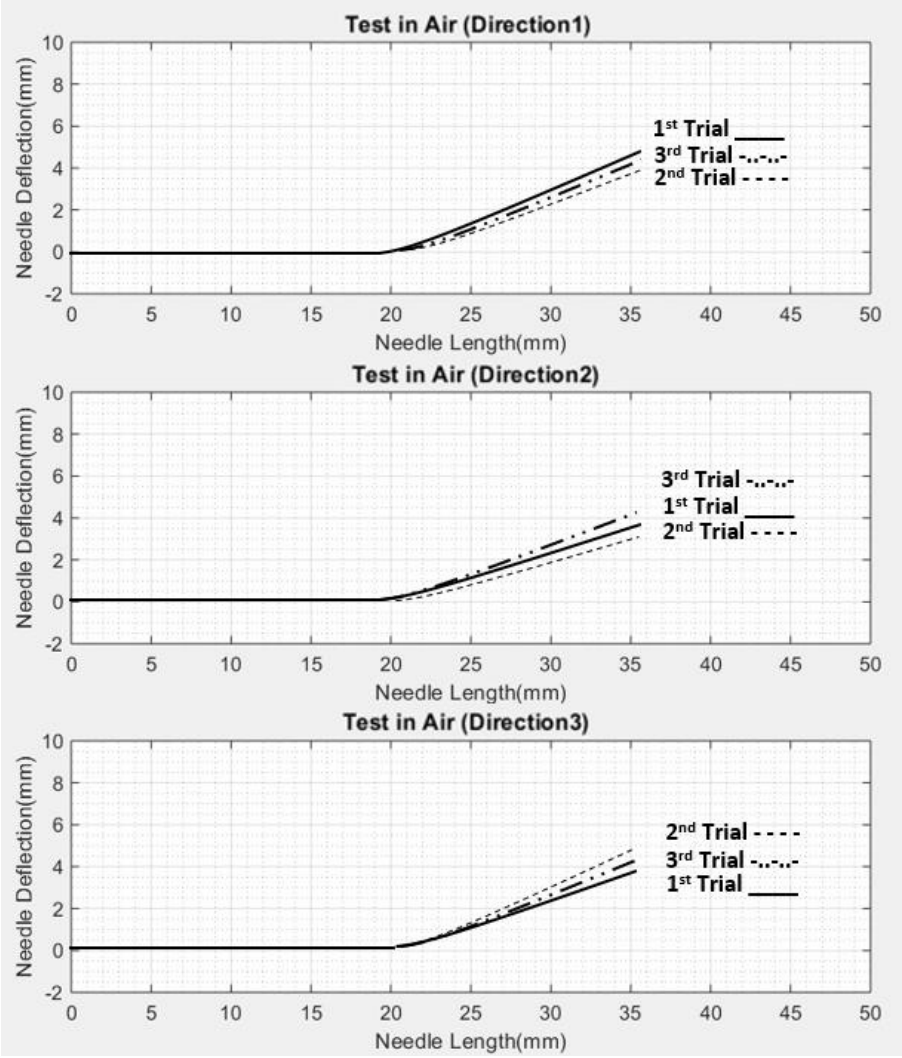

Figure 23. 3D steerable, 3D printed needle shape in air (horizontal view).

3.1.2.2. Cable-driven deflection of the 3D steerable slotted needle

In order to bend the Nitinol needle in three directions in air, as discussed in Section 3.1.1.2., a force of around 15 N should be provided by the motors. The deflection of needle tip in each direction is shown in Figure 24.

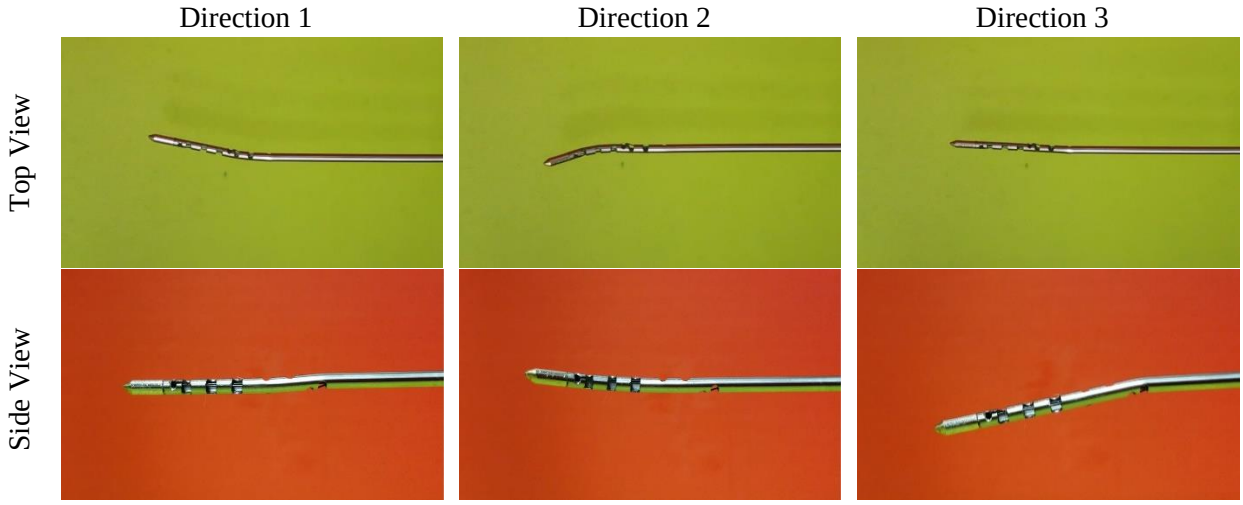

Figure 24. Top and side views of the 3D steerable slotted needle deflection in air (horizontal view).

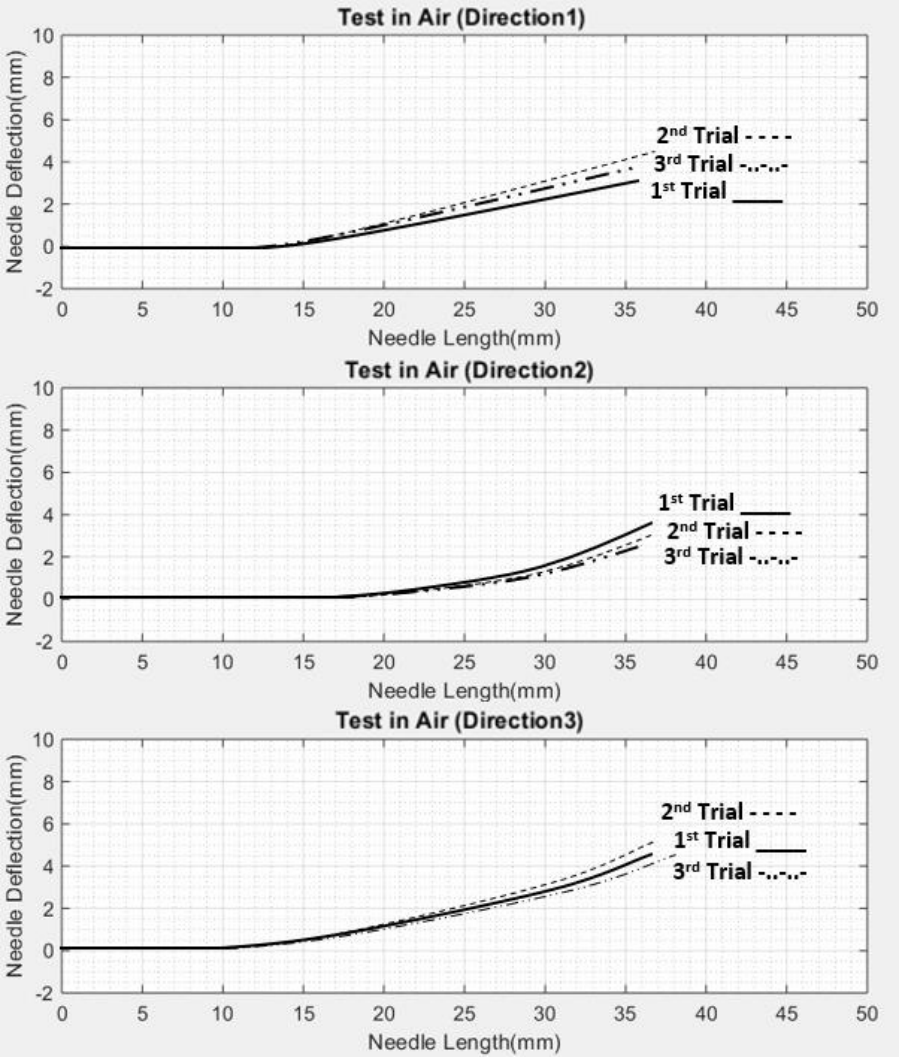

Figure 25. 3D steerable slotted needle shape in air (horizontal view).

3.1.2.3. Cable-driven deflection of the steerable active biopsy needle

The active biopsy needle is made of Nitinol and the generated force by motor was sufficient to bend the needle in three directions. Two cameras were used to capture the needle deflection as shown in Figure 26.

Figure 26. Top and side views of steerable active biopsy needle deflection in air (horizontal view).

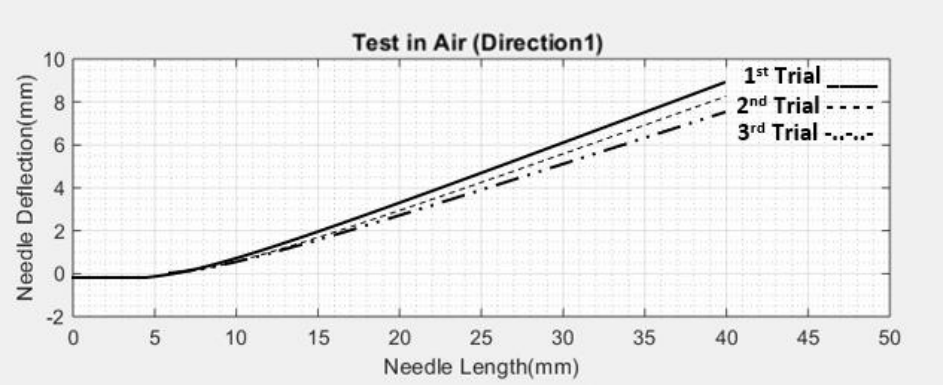

Figure 27. Steerable active biopsy needle shape in air (horizontal view).

Average needle deflection measured in this section is presented in Table 3:

Table 3. Averaged needle deflection measurement in air for three needles (horizontal view).

Angular Deflection (degree)	3D Printed Needle	Slotted Needle	Active Biopsy Needle
Direction 1	11.68±0.15 (deg.)	11.33±0.34 (deg.)	13.80±0.20 (deg.)
Direction2	11.39±0.05 (deg.)	10.15±0.06 (deg.)	N/A
Direction3	12.05±0.14 (deg.)	11.70±0.34 (deg.)	N/A
Average	11.70 (deg.)	11.06 (deg.)	13.80 (deg.)

3.2. Needles deflection in tissue

The aim of this chapter is to perform needle insertion in tissue in order to measure the needle deflection in three directions. For this purpose, a soft phantom was prepared based on the proposed method in Section 2.6. All three needles were inserted in this phantom and the amount of deflection was collected. This section introduces two procedures for testing the needles within a tissue-mimicking phantom in three directions.

3.2.1. Pulling wires

The setup that was presented in Section 2.4 is used to pull wires and makes the needle bend. This method is used to test all needles and capture the needle deflection with two cameras. The testing process is the same as Section 3.1.2 and all captures frames for three repetition are collected. It is already expected that the needle deflection in tissue decreases compared to testing in air due to tissue stiffness.

3.2.1.1. 3D steerable, 3D printed needle

The deflection of the 3D steerable, 3D printed needle (presented in Chapter 2) at its flexible joint was captured and shown in Figure 28 for three directions.

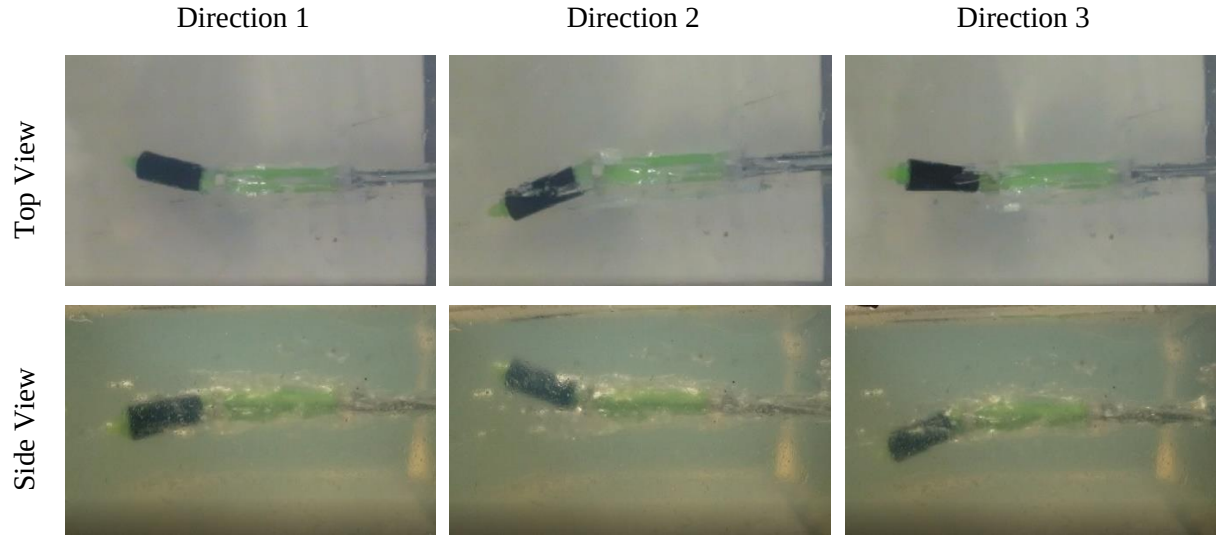

Figure 28. Top and side view of 3D steerable, 3D printed needle deflection in tissue.

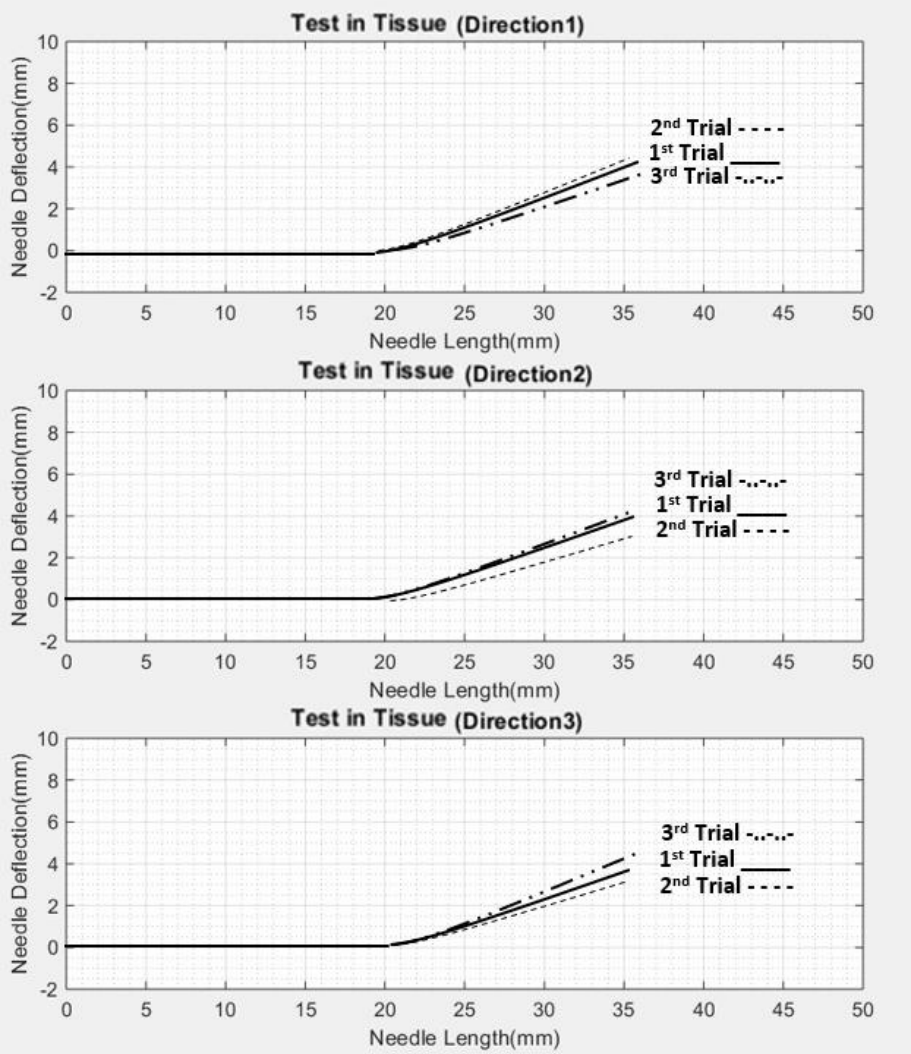

Figure 29. 3D steerable, 3D printed needle shape in tissue.

3.2.1.2. 3D steerable slotted needle

The 3D steerable slotted needle (presented in Chapter 2) was stiffer that the 3D printed needle, which may cause less angular deflection inside the tissue (Fig. 30).

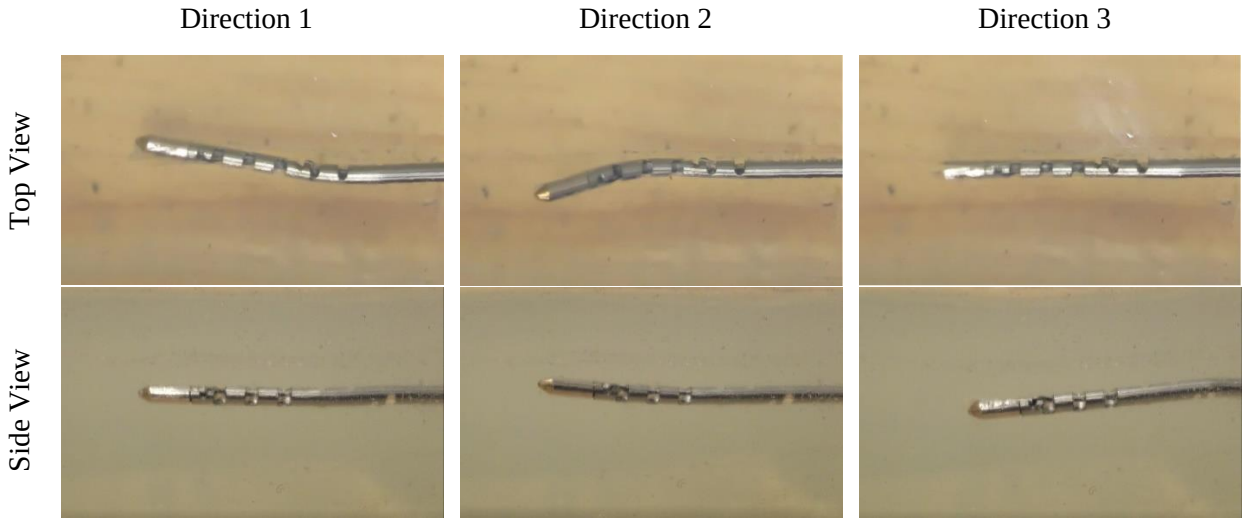

Figure 30. Top and side view of 3D steerable slotted needle deflection in tissue.

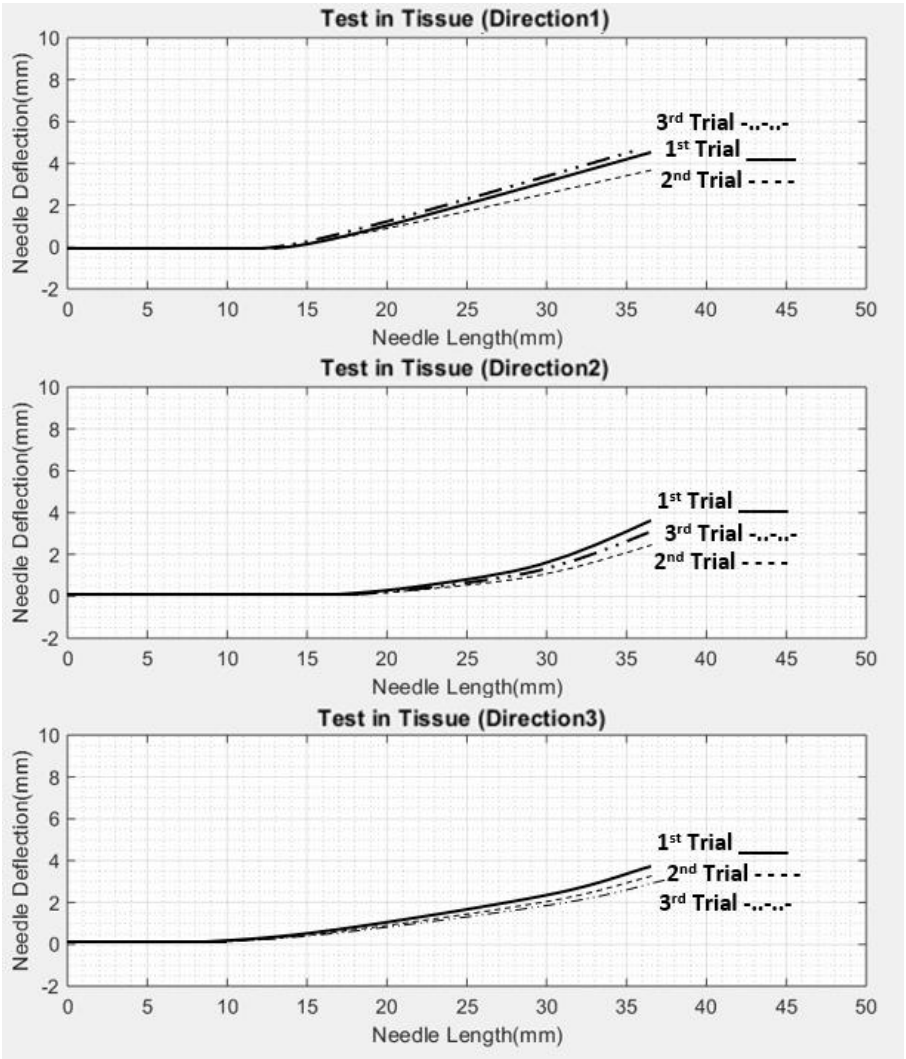

Figure 31. 3D steerable slotted needle shape in tissue.

3.2.1.3. Steerable active biopsy needle

Captured needle deflection for the steerable active biopsy Nitinol needle in three directions was captured by the cameras are shown in Figure 32.

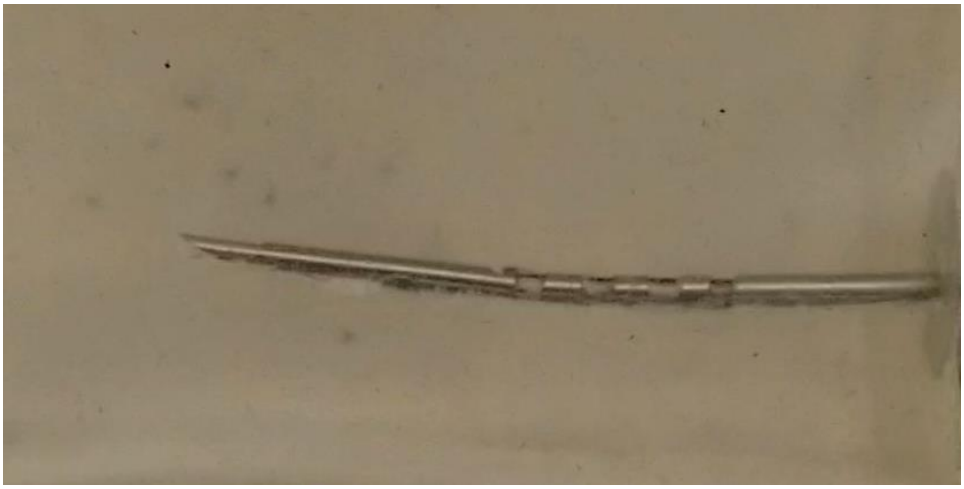

Figure 32. Top and side view of steerable active biopsy needle deflection in tissue.

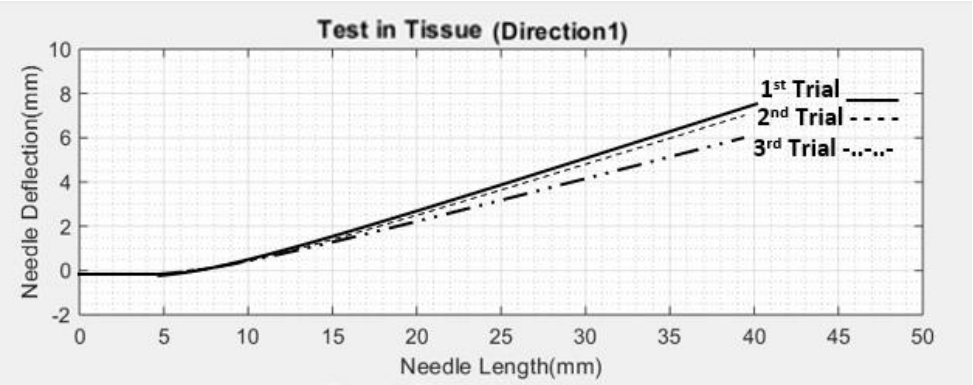

Figure 33. Steerable active biopsy needle shape in tissue.

All measurements from three repetition is demonstrated in Table 4:

Table 4. Averaged needle deflection measurement in tissue for three needles.

Angular Deflection (degree)	3D Printed Needle	Slotted Needle	Active Biopsy Needle
Direction 1	11.09±0.11 (deg.)	10.55±0.45 (deg.)	12.20±0.38 (deg.)
Direction2	10.73±0.09 (deg.)	10.01±0.01 (deg.)	N/A
Direction3	11.54±0.09 (deg.)	10.90±0.28 (deg.)	N/A
Average	11.12 (deg.)	10.49 (deg.)	12.20 (deg.)

3.2.2. Angular deflection measurement of steerable active biopsy needles and its evaluation inside tissue

Figure 34 shows the final deflection of an active needle inside the tissue phantom. The prototype was modified to have a smaller overall diameter by removing the crimps and passing the SMA wires inside holes drilled on the needle tubes. Bending was realized at the needle's flexible nylon joint (e.g., the bending section). The angular deflection was proportional to the amount of current provided to the SMA wire. Experiments showed a functional prototype of the active flexible needle operated by the integrated system. It was also concluded that the amount of force provided by the SMA actuator is sufficient to overcome the resistance of the tissue phantom and bend the needle. The defined approach to calculate the radius of curvature could be applied for the proposed active biopsy needle which bends in one direction.

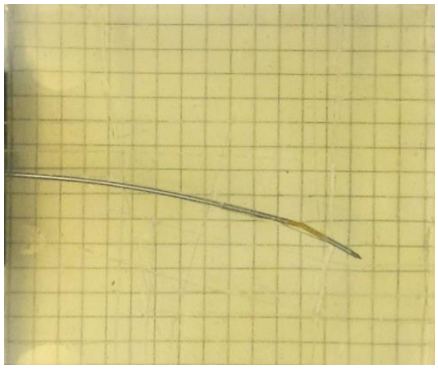

Figure 34. Active needle insertion inside a tissue phantom.

The radius of curvature was calculated for the deflected shape of the active needle. From geometric considerations (shown in Fig. 35a) we can approximate R_r (rear radius of curvature) ≈ R_f (front radius of curvature) ≈ R_α (needle tip radius of curvature) ≈ R, assuming that $L_1 \ll R$ and $L_2 \ll R$. The radius of curvature of the needle is related to φ and L_1 according to [125]:

$$R = {}^{L_1}/_{\tan(\varphi)} \tag{3.4}$$

The values for L_1 and φ are noted in Figure 35b. The angle α can be determined as:

$$\tan(\alpha) = \frac{L_1}{L_2} * \tan(\varphi) \tag{3.5}$$

the resulting radius of curvature at L_2 is determined by:

$$R_\alpha \approx R = \frac{L_2}{\sin(\alpha)} = \sqrt{L_2^2 + \left({}^{L_1}/_{\tan(\varphi)}\right)^2} \quad (3.6)$$

Substituting the values into above equations will result in the radius of curvature of 519mm at the needle tip:

$$R_\alpha \approx R = \sqrt{10^2 + \left({}^{154}/_{\tan(16.5)}\right)^2} = 519\text{mm} \quad (3.7)$$

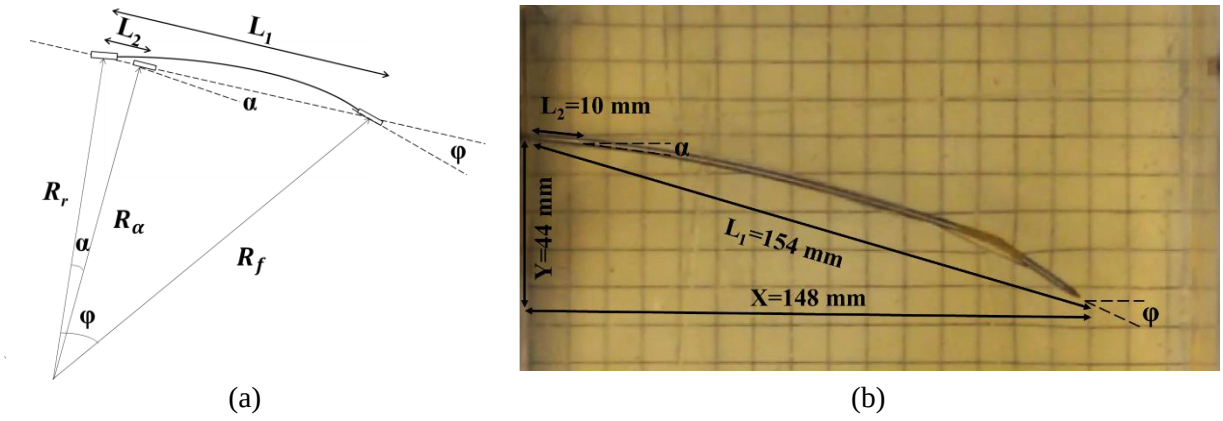

(a) (b)

Figure 35. Geometric relationship on the active needle after 150mm of axial insertion depth, and (b) dimensions.

Figure 36a shows the deflected shape of the active needle after full insertion into the tissue phantom to a depth of 150mm. Figure 36b shows the needle-tip vertical deflection versus the insertion depth. The deflection increased and with the insertion depth. Similarly, larger diameters of SMA wires require more current (power) for actuation while not resulting in a higher deflection necessarily. Based on our previous studies [110] with SMAs, the amount of force generated by the 0.2mm diameter SMA wire actuated via 1.2A the tissue (stress values at about 200MPa at the complete phase transformation) could be estimated to be about 6.3N. This amount of actuation force was sufficient for needle deflection in air and phantom. It should be noted that the higher current (i.e., 1.2A) for actuation in phantom was due to the heat loss to the surrounding tissue.

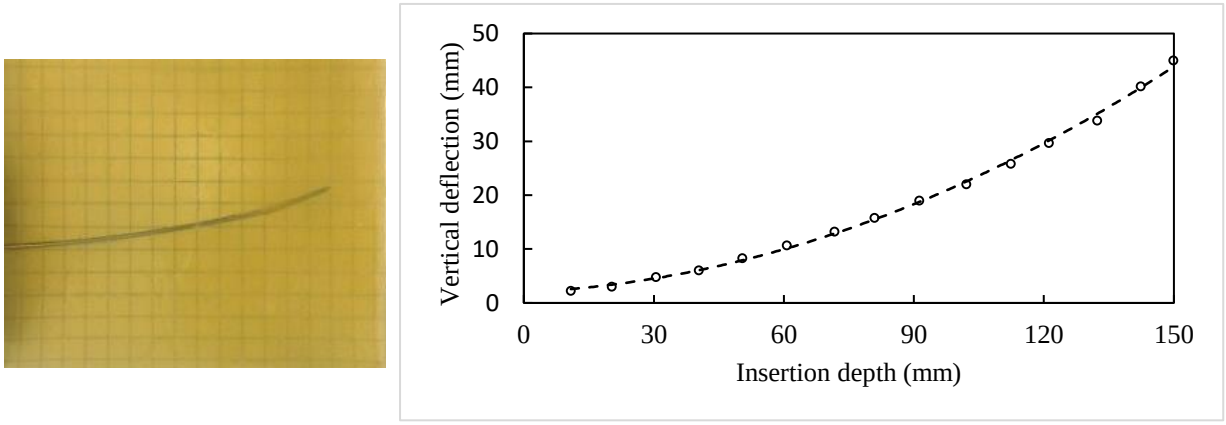

(a) (b)

Figure 36. (a) Active needle insertion, and (b) final shape of the active needle in phantom with a second-order polynomial fit.

Figure 37 shows the vertical deflection (i.e., vertical position) of the active needle tip versus insertion depth during insertion. For the first 42mm, the active needle was pushed straight into the phantom with no actuation, and thereby no vertical deflection. At this point, when the bending section of the active needle was completely located inside the phantom, the SMA wire was activated via Joule heating (providing 1.2A of current) to realize a vertical movement of about 5.1mm at the needle tip inside the phantom. The active needle was then pushed for another 108mm to the final axial depth of 150mm. The main difference between active steering and needle curving with bevel-tip needles can be seen in Figure 37 at 42mm of insertion depth. Upon actuation of SMA wire at this depth, the needle tip realized about 5.1mm of vertical movement, which is not possible via needle curving with bevel-tip needles.

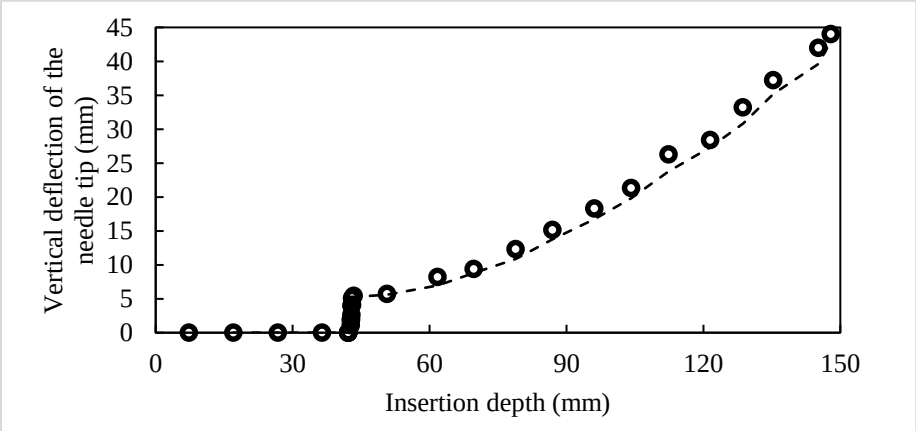

Figure 37. Vertical deflection of the active needle tip in tissue during active insertion versus insertion depth. Prototype with the Nylon joint was used here.

Figure 38 shows the vertical and horizontal position of the needle tip versus time during insertion. The needle was inserted into the phantom with no actuation for the first 8 seconds, thereby following a straight path (i.e., no vertical movement). Then SMA wire was actuated with 1.2A for 6 seconds (between 8 and 14 seconds) to realize vertical movement of 5.1mm inside the phantom. The needle was inserted for another 12 seconds to the depth of 150mm, that realized a final vertical and horizontal movement of 44 and 148mm, respectively at the needle tip.

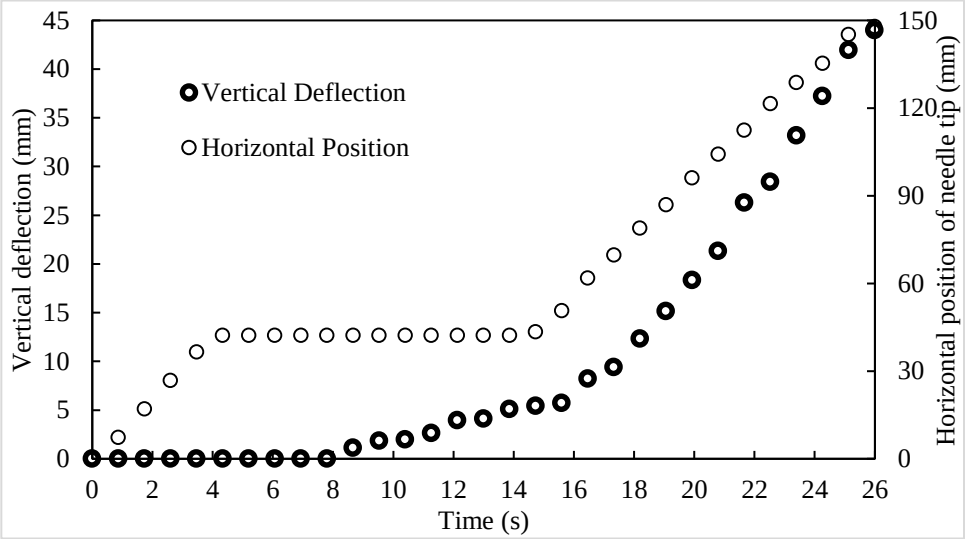

Figure 38. Vertical and horizontal position of the needle tip versus time.

3.2.3. Actuating SMA actuators

Some research groups have developed active surgical needles using SMA wires as actuators in order to navigate a needle inside tissue. As discussed in Section 1.4, SMA wires could go under a large deformation when their temperature changes. SMA wires could be activated using different methods such as conventional Joule heating [126], applying current [64], or applying electric pulses [127]. A programmable power supply (RIGOL DP832) [128] generates required constant current (with respect to the wires' resistance) to heat the wires and perform phase transformation. The measured transformation temperatures for a single SMA wire at low stress level (i.e., 15 MPa) are listed in Table 5.

Table 5. Temperature measurement of a single SMA wire at low stress level (15MPa).

	M_f (℃)	M_s (℃)	A_s (℃)	A_f (℃)
Low stress level	~25.2	~26.2	~28.8	~29.6

3.3. Motorized needle insertion

The presented method for needle insertion in a tissue-mimicking phantom is implemented based on a motorized system. This system includes two stepper motors, one of the motors provides an axial movement to steer the needle inside tissue, and the other one is embedded to enable the needle rotation (if needed). Both motors are controlled by VXM Stepping Motor Controllers which drive a motorized system including compact positioning stages and rotary tables. These components make the positioning stages easier and more effective.

Motorized needle insertion is beneficial for those surgeries that need to be operated remotely because the entire process is controlled by a MATLAB code with no hand interference. In addition, it increases needle steerability. Moreover, a telescopic radio antenna is attached to a partition and supports the needle to be directly inserted in tissue as motor provides forward motion.

Using the provided needle insertion setup in Section 2.3., MATLAB code commands stepper motors to steer needle for a precise insertion inside the prepared phantom and increase targeting. The needle is passed through center aperture (hollow spindle) on the motorized rotary table, which is mounted horizontally, and is secured by tightening embedded screws on the rotary table.

Furthermore, a partition is located at the end of the horizontal positioning stage to separate motor and phantom. The tissue is also elevated up to the right height at the other side of partition so that the needle will be completely inside the phantom during insertion.

Three proposed needles are tested using the motorized system to evaluate needle deflection in 3D. The needle curvature is captured using two cameras as well as the transducer connected to ultrasound machine. This section demonstrates and analyzes captured deflections by cameras only, and next section will discuss about captured frames by ultrasound probe. Additionally, a comparison between obtained result in this part and the ones in Section 3.1.2. for all needles in 3D is provided as Table 6.

Table 6. Averaged needle deflection measurement in tissue for three needles using motorized system.

Angular Deflection (degree)	3D Printed Needle	Slotted Needle	Active Biopsy Needle
Direction 1	11.01±0.14 (deg.)	10.49±0.25 (deg.)	13.83±0.29 (deg.)
Direction2	10.95±0.21 (deg.)	10.35±0.40 (deg.)	N/A
Direction3	11.15±0.02 (deg.)	10.60±0.10 (deg.)	N/A
Average	11.03 (deg.)	10.48 (deg.)	13.83 (deg.)

3.4. Tracking the needle tip via ultrasound device

Many of the needle insertions are being performed under ultrasound guidance for research or treatment purposes. An effective image-guided needle insertion depends on the clarity of the needle location and accurate tracking. In general, ultrasound tracking is known as a robust technique to detect and track the needle tip in tissue. Some methods have been suggested to improve estimations of the needle position in real time inside the tissue. Such methods include needle trajectory calculation and markings with a single camera attached to the ultrasound transducer [129], Optical Flow-Based in-plane tracking algorithm [130], ROI-RK method (which is tracking Region of Interest based on RANSAC algorithm) and Kalman Filter [131]. In this work, a method based on iterative clustering has been used to track the needle trajectory [132],[133].

Using a 2D ultrasound probe, needle trajectory in three directions for the three needles was investigated and captured. In order to move the probe automatically forward/backward or side to side, two stepper motors were mounted above phantom including two positioning stages in X-Y plane. There are two approaches defined by orientation of needle with respect to ultrasound transducer to track the needle trajectory inside tissue.

3.4.1. Parallel technique (azimuthal or longitudinal approach)

The probe is located parallel to the needle to visualize the entire length of needle that is inserted in tissue. This is advantageous for needle tip tracking at all times to ensure that the needle is completely inside tissue. Additionally, the needle penetration inside tissue during interventional procedures increases. On other hand, this approach is challenging since the needle should be kept under a very thin ultrasound beam. This approach is used to track the needle tip and visualize path trajectory in three directions for the three designed needles.

3.4.2. Perpendicular technique (transverse approach)

The probe is positioned perpendicular to the needle to visualize the needle's cross section as a "dot" sign within tissue. Since the needle is passed through a large section of ultrasound beam, this approach does not have the challenge of the parallel technique. The needle penetrates less compare to the parallel technique. In addition, the needle visualization is limited because a cross section of the needle tip is captured at any time.

As mentioned earlier, this section introduces a new method to track the needle tip precisely inside the tissue-mimicking phantom to improve targeting. As shown in Figure 39, a yellow marker

represents the tip of needle tracked by Simple Linear Iterative Clustering (SLIC) superpixels method [132]. Superpixels were generated in this method followed by a 2D Kalman filter to predict the needle tip location based on its previously tracked frames [133]. About 400 frames were captured (two trails with 200 frames each) from the needle insertion in two phantoms with different qualities to demonstrate the accuracy of this needle tip tracking method. The tracking method resulted in zero and 32 lost frames in the High- and Low-quality phantom, respectively. It indicated that phantom structure significantly affects the tracking results. The lost frames resulted from the bubbles in the Low-quality phantom that led into needle invisibility in some parts of insertion (Fig. 39 (b) and (c)). As shown in Figure 39 (b), the tip of the needle was inside the drawn red box where it was not visible for consecutive frames until it suddenly reappeared in the next frame in Figure 39 (c). This issue did not occur during insertion in the High-quality phantom which had almost no bubbles (Fig. 39 (e) and (f)).

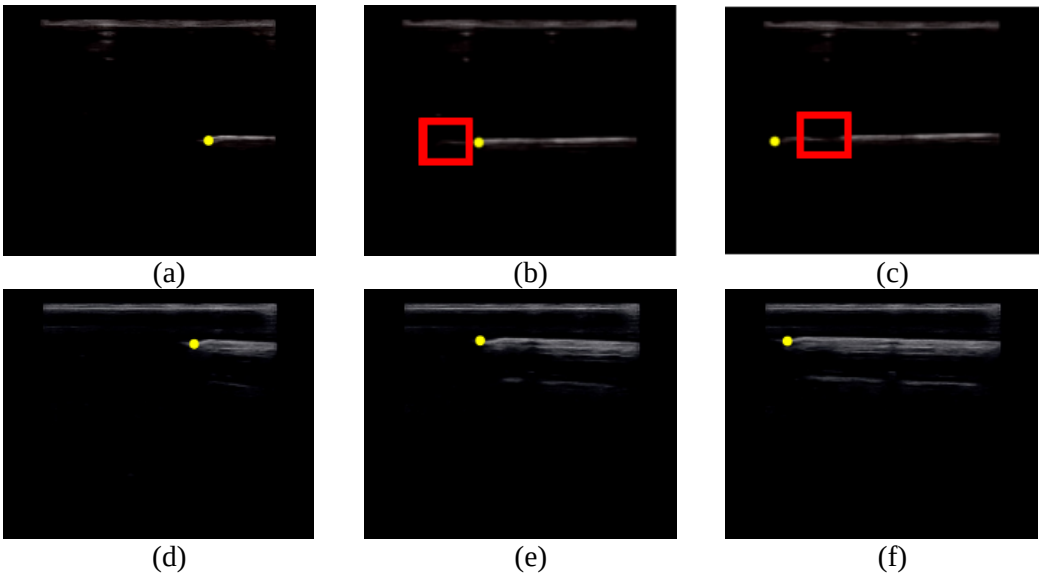

Figure 39. Needle insertion tracking (a) entry, (b) mid, (c) late insertion points in low-quality phantom, (d) entry, (e) mid, (f) late insertion point in high-quality phantom.

Generally, in comparison with CT-Scan, MRI, and X-ray, ultrasound guidance is more appropriate to track needle trajectory because it provides a real-time imaging modality. In addition, it does not involve the use of ionizing radiation which protects patients undergoing repeated exposures and makes it applicable for intra-operative and intra-procedural image-guided procedures for clinicians. Moreover, to steer the needle in a desired trajectory into a region of interest to perform biopsy or excision of target tissue, ultrasound imaging guidance is widely

recommended. Considering all of these advantages of using ultrasound-guided methods, this study suggested methods for improved visualization of the needle tip inside phantom materials for a reliable needle tracking.

CONCLUSION

Percutaneous needle-based procedures are known as a popular minimally invasive technique that are being used in therapeutic and diagnostic procedures. Today, brachytherapy, biopsy, ablations and lumpectomy are performed via surgical needles. The success of these procedures highly depends on the accuracy of needle placement at target positions. During the past several years, research groups have suggested methods to improve the needle guidance towards the target locations. Flexible passive and active needles have been suggested for improved steerability inside the tissue. Passive needles use the unbalanced forces at their tip, while active needles are utilizing an external source of bending force to follow a desired trajectory. Although promising, neither of passive nor active needle designs have been used in clinical practice. Most of the active needle designs to date can realize deflection in only one direction. The needle rotation then can be used to reach the targets in 3D locations. Rotation of the needle can cause extra damage to the tissue, that should be avoided. This work introduced three distinct needle designs to realize needle deflection in multiple directions. The first needle was designed with a scale usable for lumpectomy that was fabricated via 3D printing process. The second needle was designed with three set of slots arranged 120 degrees evenly. This needle was made for brachytherapy procedure. The third needle was specifically made for tissue biopsy with one set of slits to realize one degree of freedom manipulation. The needles were tested in air and tissue to demonstrate their functionality as a feasibility study. In conclusion, about 11 degrees of angular deflection was realized in multiple directions via three needle prototypes in air and in tissue-mimicking phantom. This amount of angular deflection is expected to be used in needle-based procedures in a curvilinear method to enhance the accuracy and minimize trauma to the tissue.

To control the deflection a motorized system was developed to manipulate the needles via tendon cables. The programmed stepper motors were used to control the needle curvature at a desired angular deflection. This motorized system could be used on a robotic needle insertion system to combine angular deflection with needle's axial and rotational movements to steer the needle in an effective way towards the target. The robotic needle insertion system is equipped with ultrasound tracking device to track the needle tip during needle steering. In conclusion, this work also showed an effective way for robotic needle insertion and to use the ultrasound imaging to locate the needle. In future works, the modules that are developed (i.e., the active needles and ultrasound tracking) and studied (i.e., the deflection analyses) in this work will integrate with other

robotic modules of our robotic needle insertion system, and when properly programmed, the system can perform an automated needle insertion towards the target. In Addition, finite element analysis using COMSOL will be performed for design optimization and fatigue analysis. Steerable biopsy needle will also be modified to bend in three directions.

REFERENCES

[1] "Leading Causes of Death," *Centers for Disease Control and Prevention*. [Online]. Available: https://www.cdc.gov/nchs/fastats/leading-causes-of-death.htm. [Accessed: 14-Dec-2019].

[2] "Common Cancer Types," *National Cancer Institute*. [Online]. Available: https://www.cancer.gov/types/common-cancers. [Accessed: 14-Dec-2019].

[3] "Estimated New Cases of Breast Cancer," *American Cancer Society/Cancer Statistics Center/Breast*. [Online]. Available: https://cancerstatisticscenter.cancer.org/#!/cancer-site/Breast. [Accessed: 14-Dec-2019].

[4] "Estimated New Cases of Prostate Cancer," *American Cancer Society/Cancer Statistics Center/Prostate*. [Online]. Available: https://cancerstatisticscenter.cancer.org/#!/cancer-site/Prostate. [Accessed: 14-Dec-2019].

[5] K. B. Reed, A. M. Okamura, and N. J. Cowan, "Modeling and control of needles with torsional friction," *IEEE Trans. Biomed. Eng.*, vol. 56, no. 12, pp. 2905-2916, 2009.

[6] V. Duindam, R. Alterovitz, S. Sastry, and K. Goldberg, "Screw-based motion planning for bevel-tip flexible needles in 3D environments with obstacles," in *Proceedings - IEEE International Conference on Robotics and Automation*, pp. 2483-2488, 2008.

[7] S. P. DiMaio and S. E. Salcudean, "Needle steering and model-based trajectory planning," *Lect. Notes Comput. Sci. (including Subser. Lect. Notes Artif. Intell. Lect. Notes Bioinformatics)*, pp. 33-40, 2003.

[8] M. Torabi, K. Hauser, R. Alterovitz, V. Duindam, and K. Goldberg, "Guiding medical needles using single-point tissue manipulation," in *Proceedings - IEEE International Conference on Robotics and Automation*, pp. 2705-2710, 2009.

[9] S. P. Dimaio and S. E. Salcudean, "Needle steering and motion planning in soft tissues," *IEEE Transactions on Biomedical Engineering*. vol. 52, no. 6, pp. 965-974, 2005.

[10] R. Alterovitz, M. Branicky, and K. Goldberg, "Motion planning under uncertainty for image-guided medical needle steering," in *International Journal of Robotics Research*, vol. 27, no. 11-12, pp. 1361-1374, 2008.

[11] M. Abayazid, R. J. Roesthuis, R. Reilink, and S. Misra, "Integrating deflection models and image feedback for real-time flexible needle steering," *IEEE Trans. Robot.*, vol. 29, no. 2, pp. 542-553, 2013.

[12] Z. Neubach and M. Shoham, "Ultrasound-guided robot for flexible needle steering," *IEEE Trans. Biomed. Eng.*, vol. 57, no. 4, pp. 799-805, 2010.

[13] R. Alterovitz, T. Siméon, and K. Goldberg, "The stochastic motion roadmap: A sampling framework for planning with Markov motion uncertainty ," in *Robotics: Science and Systems*, pp. 75-89, 2008.

[14] S. Patil, J. Burgner, R. J. Webster, and R. Alterovitz, "Needle steering in 3-D Via rapid replanning," *IEEE Trans. Robot.*, vol. 30, no. 4, pp. 853-864, 2014.

[15] D. Glozman and M. Shoham, "Image-guided robotic flexible needle steering," *IEEE Trans. Robot.*, vol. 23, no. 3, pp. 459-467, 2007.

[16] K. B. Reed *et al.*, "Robot-assisted needle steering," *IEEE Robot. Autom. Mag.*, vol. 18, no. 4, pp. 35-46, 2011.

[17] M. S. Apaydin, D. L. Brutlag, C. Guestrin, D. Hsu, J. C. Latombe, and C. Varma, "Stochastic Roadmap Simulation: An Efficient Representation and Algorithm for Analyzing Molecular Motion," in *Journal of Computational Biology*, vol. 10, no. 3-4, pp. 257-281, 2003.

[18] M. S. Apaydin, D. L. Brutlag, C. Guestrin, D. Hsu, and J. C. Latombe, "Stochastic conformational roadmaps for computing ensemble properties of molecular motion," in *Springer Tracts in Advanced Robotics*, pp. 1-17, 2004.

[19] R. Alterovitz, K. Goldberg, and A. Okamura, "Planning for steerable bevel-tip needle insertion through 2D soft tissue with obstacles," in *Proceedings - IEEE International Conference on Robotics and Automation*, pp. 1640-1645, 2005.

[20] K. Hauser, R. Alterovitz, N. Chentanez, A. Okamura, and K. Goldberg, "Feedback control for steering needles through 3D deformable tissue using helical paths," in *Robotics: Science and Systems*, vol. 37, pp. 1-23, 2009.

[21] R. J. Webster, N. J. Cowan, G. Chirikjian, and A. M. Okamura, "Nonholonomic modeling of needle steering," *Springer Tracts Adv. Robot.*, vol. 25, no. 5-6, pp. 509-525, 2006.

[22] W. Liang, Y. Huang, Y. Xu, R. K. Lee, and A. Yariv, "Highly sensitive fiber Bragg grating refractive index sensors," *Appl. Phys. Lett.*, vol. 86, no. 15, pp. 1-3, 2005.

[23] M. Abayazid, M. Kemp, and S. Misra, "3D flexible needle steering in soft-tissue phantoms using Fiber Bragg Grating sensors," in *Proceedings - IEEE International Conference on Robotics and Automation*, pp. 5823-5829, 2013.

[24] R. J. Roesthuis, M. Kemp, J. J. Van Den Dobbelsteen, and S. Misra, "Three-dimensional needle shape reconstruction using an array of fiber bragg grating sensors," *IEEE/ASME Trans. Mechatronics*, vol. 19, no. 4, pp. 1115-1126, 2014.

[25] N. Abolhassani, R. Patel, and M. Moallem, "Needle insertion into soft tissue: A

survey," *Med. Eng. Phys.*, vol. 29, no. 4, pp. 413-431, 2007.

[26] C. Simone and A. M. Okamura, "Modeling of needle insertion forces for robot-assisted percutaneous therapy," in *Proceedings - IEEE International Conference on Robotics and Automation*, vol. 2, pp. 2085-2091, 2002.

[27] P. N. Brett, C. A. Fraser, M. Hennigan, M. V. Griffiths, and Y. Kamel, "Automatic Surgical Tools for Penetrating Flexible Tissues," *IEEE Eng. Med. Biol. Mag.*, vol. 14, no. 3, pp. 264-270, 1995.

[28] P. N. Brett, A. J. Harrison, and T. A. Thomas, "Schemes for the identification of tissue types and boundaries at the tool point for surgical needles," *IEEE Trans. Inf. Technol. Biomed.*, vol. 4, no. 1, pp. 30-36, 2000.

[29] S. Misra, K. T. Ramesh, and A. M. Okamura, "Modeling of tool-tissue interactions for computer-based surgical simulation: A literature review," *Presence Teleoperators Virtual Environ.*, vol. 17, no. 5, pp. 463-491, 2008.

[30] N. V. Datla *et al.*, "A model to predict deflection of bevel-tipped active needle advancing in soft tissue," *Med. Eng. Phys.*, vol. 36, no. 3, pp. 285-293, 2014.

[31] R. J. Roesthuis, Y. R. J. Van Veen, A. Jahya, and S. Misra, "Mechanics of needle-tissue interaction," in *IEEE International Conference on Intelligent Robots and Systems*, pp. 2557-2563, 2011.

[32] R. J. Roesthuis, M. Abayazid, and S. Misra, "Mechanics-based model for predicting in-plane needle deflection with multiple bends," in *Proceedings of the IEEE RAS and EMBS International Conference on Biomedical Robotics and Biomechatronics*, pp. 69-74, 2012.

[33] N. Abolhassani and R. V. Patel, "Deflection of a flexible needle during insertion into soft tissue," in *Annual International Conference of the IEEE Engineering in Medicine and Biology - Proceedings*, vol. 1, pp. 3858-3861, 2006.

[34] H. Kataoka, T. Washio, M. Audette, and K. Mizuhara, "A model for relations between needle deflection, force, and thickness on needle penetration," in *Lecture Notes in Computer Science*, pp. 966-974, 2001.

[35] J. T. Hing, A. D. Brooks, and J. P. Desai, "Reality-based needle insertion simulation for haptic feedback in prostate brachytherapy," in *Proceedings - IEEE International Conference on Robotics and Automation*, pp. 619-624, 2006.

[36] H. W. Nienhuys and A. F. Van Der Stappen, "A computational technique for interactive needle insertions in 3D nonlinear material," in *Proceedings - IEEE International Conference on Robotics and Automation*, vol. 2, pp. 2061-2067, 2004.

[37] K. G. Yan, T. Podder, Y. Yu, T. I. Liu, C. W. S. Cheng, and W. S. Ng, "Flexible

needle-tissue interaction modeling with depth-varying mean parameter: Preliminary study," *IEEE Trans. Biomed. Eng.*, vol. 56, no. 2, pp. 255-262, 2009.

[38] R. Alterovitz, K. Goldberg, J. Pouliot, R. Taschereau, and I. C. Hsu, "Needle insertion and radioactive seed implantation in human tissues: Simulation and sensitivity analysis," in *Proceedings - IEEE International Conference on Robotics and Automation*, vol. 2, pp. 1793-1799, 2003.

[39] T. Yang, H. Yin, X. Zhao, J. Han, and W. Xu, "Interaction modeling and simulation of a flexible needle insertion into soft tissues," in *Proceedings for the Joint Conference of ISR - 41th International Symposium on Robotics and Robotik, ISR/ROBOTIK*, 2014.

[40] J. R. Crouch, C. M. Schneider, J. Wainer, and A. M. Okamura, "A velocity-dependent model for needle insertion in soft tissue," in *Lecture Notes in Computer Science (including subseries Lecture Notes in Artificial Intelligence and Lecture Notes in Bioinformatics)*, vol. 8, no. 2, pp. 624-632, 2005.

[41] M. Heverly, P. Dupont, and J. Triedman, "Trajectory optimization for dynamic needle insertion," in *Proceedings - IEEE International Conference on Robotics and Automation*, pp. 1646-1651, 2005.

[42] N. V. Datla, B. Konh, and P. Hutapea, "A flexible active needle for steering in soft tissues," in *Proceedings of the IEEE Annual Northeast Bioengineering Conference, NEBEC*, pp. 1-2, 2014.

[43] S. C. Ryu, P. Renaud, R. J. Black, B. L. Daniel, and M. R. Cutkosky, "Feasibility study of an optically actuated MR-compatible active needle," in *IEEE International Conference on Intelligent Robots and Systems*, pp. 2564-2569, 2011.

[44] S. C. Ryu *et al.*, "Design of an optically controlled MR-compatible active needle," *IEEE Trans. Robot.*, vol. 31, no. 1, pp. 1-11, 2015.

[45] S. C. Ryu, Z. F. Quek, P. Renaud, R. J. Black, B. L. Daniel, and M. R. Cutkosky, "An optical actuation system and curvature sensor for a MR-compatible active needle," in *Proceedings - IEEE International Conference on Robotics and Automation*, pp. 1589-1594, 2012.

[46] D. C. Lagoudas, "Shape Memory Alloys, Modeling and Engineering Applications," *Springer US*, 2008.

[47] M. H. Elahinia, "Shape memory alloy actuators: design, fabrication, and experimental evaluation," *Wiley*, 2016.

[48] J. Mohd Jani, M. Leary, A. Subic, and M. A. Gibson, "A review of shape memory alloy research, applications and opportunities," *Materials and Design*. vol. 56, pp. 1078-1113, 2014.

[49] L. Case, “Shape Memory Alloy Shape Training Tutorial,” *Transformation*, 2004.

[50] L. Lecce and A. Concilio, “Shape Memory Alloy Engineering,” *Elsevier Science*, 2015.

[51] “Memry Corporation.” [Online]. Available: https://www.memry.com/#nitinol.

[52] Z. Lekston and E. Łągiewka, “X-ray diffraction studies of NiTi shape memory alloys,” *Arch. Mater. Sci.*, vol. 28, no. 11, pp. 665-672, 2007.

[53] J. Uchil, F. M. B. Fernandes, and K. K. Mahesh, “X-ray diffraction study of the phase transformations in NiTi shape memory alloy,” *Mater. Charact.*, vol. 58, no. 3, pp. 243-248, 2007.

[54] M. Honarvar, B. Konh, T. K. Podder, A. P. Dicker, Y. Yu, and P. Hutapea, “X-ray Diffraction Investigations of Shape Memory NiTi Wire,” *J. Mater. Eng. Perform.*, vol. 24, no. 8, pp. 3038-3048, 2015.

[55] L. Petrini and F. Migliavacca, “Biomedical Applications of Shape Memory Alloys,” *J. Metall.*, pp. 1-15, 2011.

[56] N. B. Morgan, “Medical shape memory alloy applications - The market and its products,” *Mater. Sci. Eng. A*, vol. 378, no. 1, pp. 16-23, 2004.

[57] D. Tarniţă, D. N. Tarniţă, N. Bîzdoacă, I. Mîndrilă, and M. Vasilescu, “Properties and medical applications of shape memory alloys,” *Rom. J. Morphol. Embryol.*, vol. 50, no. 1, pp. 15–21, 2009.

[58] L. G. Machado and M. A. Savi, “Medical applications of shape memory alloys,” *Brazilian Journal of Medical and Biological Research*., vol. 36, no. 6, pp. 683-691, 2003.

[59] M. Honarvar *et al.*, “Study of unrecovered strain and critical stresses in one-way shape memory Nitinol,” *J. Mater. Eng. Perform.*, vol. 23, no. 8, pp. 2885-2893, 2014.

[60] K. Tanaka, “Thermomechanical Sketch of Shape Memory Effect: One-Dimensional Tensile Behavior.,” *Res Mech. Int. J. Struct. Mech. Mater. Sci.*, vol. 18, no. 3, pp. 251–263, 1986.

[61] C. Liang and C. A. Rogers, “One-Dimensional Thermomechanical Constitutive Relations for Shape Memory Materials,” *J. Intell. Mater. Syst. Struct.*, vol. 8, no. 4, pp. 285-302, 1997.

[62] L. C. Brinson, “One-dimensional constitutive behavior of shape memory alloys: Thermomechanical derivation with non-constant material functions and redefined martensite internal variable,” *J. Intell. Mater. Syst. Struct.*, vol. 4, no. 2, pp. 229–242, 1993.

[63] H. Prahlad and I. Chopra, “Comparative evaluation of shape memory alloy constitutive models with experimental data,” *J. Intell. Mater. Syst. Struct.*, vol. 12, no. 6, pp. 383–395, 2001.

[64] N. V Datla, B. Konh, and P. Hutapea, “Studies with SMA actuated needle for steering within tissue,” in *ASME Conf. on Smart Material, Adaptive Structures and Intelligent Systems (SMASIS)*, pp. 1–4, 2014.

[65] B. Konh and T. K. Podder, “Design and Fabrication of a Robust Active Needle using SMA Wires,” in *DMD Conf.*, pp. 1-2, 2017.

[66] B. Konh, M. Honarvar, and P. Hutapea, “Design optimization study of a shape memory alloy active needle for biomedical applications,” *Med. Eng. Phys.*, vol. 37, no. 5, pp. 469-477, 2015.

[67] B. Konh, “SMART SURGICAL NEEDLE ACTUATED BY SHAPE MEMORY ALLOYS FOR PERCUTENEOUS PROCEDURES,” A Dissertation Submitted to the Temple University Graduate Board In Partial Fulfillment of the Requirements for the Degree DOCTOR OF PHILOSOPHY by Bardia Konh May 2016 Exami, 2016.

[68] F. O. M. Joseph *et al.*, “Development of a coordinated controller for robot-assisted shape memory alloy actuated needle for prostate brachytherapy,” *36th Annual International Conference of the IEEE Engineering in Medicine and Biology Society, EMBC*, pp. 357-360, 2014.

[69] F. O. M. Joseph *et al.*, “Control of Shape Memory Alloy Actuated Flexible Needle Using Multimodal Sensory Feedbacks,” *J. Autom. Control Eng.*, pp. 428-434, 2015.

[70] M. Honarvar, B. Konh, and P. Hutapea, “Investigation of crystal structures of one-way shape memory Nitinol wire actuators for active steerable needle,” in *Behavior and Mechanics of Multifunctional Materials and Composites*, pp. 1-10, 2015.

[71] M. H. Elahinia and H. Ashrafiuon, “Nonlinear control of a shape memory alloy actuated manipulator,” *J. Vib. Acoust. Trans. ASME*, vol. 124, no. 4, pp. 566-576, 2002.

[72] R. D. Bucholz and K. A. Laycock, “Image-guided surgery,” in *Biomedical Photonics: Handbook*, 2003.

[73] K. B. Reed, V. Kallem, R. Alterovitzt, K. Goldberg, A. M. Okamura, and N. J. Cowan, “Integrated planning and image-guided control for planar needle steering,” in *Proceedings of the 2nd Biennial IEEE/RAS-EMBS International Conference on Biomedical Robotics and Biomechatronics, BioRob*, pp. 819-824, 2008.

[74] P. J. Swaney *et al.*, “Tracked 3D ultrasound targeting with an active cannula,” in *Medical Imaging 2012: Image-Guided Procedures, Robotic Interventions, and*

Modeling, pp. 1-9, 2012.

[75] J. Hong, T. Dohi, M. Hashizume, K. Konishi, and N. Hata, "An ultrasound-driven needle-insertion robot for percutaneous cholecystostomy," *Phys. Med. Biol.*, vol. 49, no. 3, pp. 441-455, 2004.

[76] G. J. Vrooijink, M. Abayazid, and S. Misra, "Real-time three-dimensional flexible needle tracking using two-dimensional ultrasound," in *Proceedings - IEEE International Conference on Robotics and Automation*, pp. 1680-1685, 2013.

[77] G. J. Vrooijink, M. Abayazid, S. Patil, R. Alterovitz, and S. Misra, "Needle path planning and steering in a three-dimensional non-static environment using two-dimensional ultrasound images," *Int. J. Rob. Res.*, vol. 33, no. 10, pp. 1361-1374, 2014.

[78] M. Ding, H. N. Cardinal, and A. Fenster, "Automatic needle segmentation in three-dimensional ultrasound images using two orthogonal two-dimensional image projections," *Med. Phys.*, vol. 30, no. 2, pp. 222-234, 2003.

[79] A. Pourtaherian, S. Zinger, P. H. N. De With, H. H. M. Korsten, and N. Mihajlovic, "Gabor-based needle detection and tracking in three-dimensional ultrasound data volumes," in *2014 IEEE International Conference on Image Processing, ICIP*, pp. 3602-3606, 2014.

[80] M. Abayazid, G. J. Vrooijink, S. Patil, R. Alterovitz, and S. Misra, "Experimental evaluation of ultrasound-guided 3D needle steering in biological tissue," *Int. J. Comput. Assist. Radiol. Surg.*, vol. 9, no. 6, pp. 931-939, 2014.

[81] M. Abayazid, P. Moreira, N. Shahriari, S. Patil, R. Alterovitz, and S. Misra, "Ultrasound-guided three-dimensional needle steering in biological tissue with curved surfaces," *Med. Eng. Phys.*, vol. 37, no. 1, pp. 145-150, 2015.

[82] T. Ungi *et al.*, "Spinal needle navigation by tracked ultrasound snapshots," *IEEE Trans. Biomed. Eng.*, vol. 59, no. 10, pp. 2766-2772, 2012.

[83] P. Chatelain, A. Krupa, and M. Marchal, "Real-time needle detection and tracking using a visually servoed 3D ultrasound probe," in *Proceedings - IEEE International Conference on Robotics and Automation*, pp. 1668-1673, 2013.

[84] E. M. Boctor *et al.*, "Precisely shaped acoustic ablation of tumors utilizing steerable needle and 3D ultrasound image guidance," in *Medical Imaging 2010: Visualization, Image-Guided Procedures, and Modeling*, pp. 1-10, 2010.

[85] E. M. Boctor, M. A. Choti, E. C. Burdette, and R. J. Webster, "Three-dimensional ultrasound-guided robotic needle placement: An experimental evaluation," *Int. J. Med. Robot. Comput. Assist. Surg.*, vol. 4, no. 2, pp. 180-191, 2008.

[86] D. Stoianovici, L. L. Whitcomb, J. H. Anderson, R. H. Taylor, and L. R. Kavoussi,

"A modular surgical robotic system for image guided percutaneous procedures," in *Lecture Notes in Computer Science*, pp. 404-410, 1998.

[87] E. M. Boctor, R. J. Webster, M. A. Choti, R. H. Taylor, and G. Fichtinger, "Robotically assisted ablative treatment guided by freehand 3D ultrasound," *Int. Congr. Ser.*, pp. 503-508, 2004.

[88] T. K. Adebar, A. E. Fletcher, and A. M. Okamura, "3-D ultrasound-guided robotic needle steering in biological tissue," *IEEE Trans. Biomed. Eng.*, vol. 61, no. 12, pp. 2899-2910, 2014.

[89] T. K. Adebar and A. M. Okamura, "3D segmentation of curved needles using Doppler ultrasound and vibration," in *Lecture Notes in Computer Science*, pp.1-7, 2013.

[90] J. D. Greer, T. K. Adebar, G. L. Hwang, and A. M. Okamura, "Real-time 3D curved needle segmentation using combined B-mode and power Doppler ultrasound," *Med. Image Comput. Comput. Assist. Interv.*, vol. 17, no. 2, pp. 381-388, 2014.

[91] M. Waine, C. Rossa, R. Sloboda, N. Usmani, and M. Tavakoli, "Needle Tracking and Deflection Prediction for Robot-Assisted Needle Insertion Using 2D Ultrasound Images," *J. Med. Robot. Res.*, vol. 1, no. 1, pp. 1-11, 2016.

[92] S. W. Wong, A. U. Niazi, K. J. Chin, and V. W. Chan, "Real-time ultrasound-guided spinal anesthesia using the SonixGPS® needle tracking system: A case report," *Can. J. Anesth.*, vol. 60, no. 1, pp. 50-53, 2013.

[93] A. U. Niazi, K. J. Chin, R. Jin, and V. W. Chan, "Real-time ultrasound-guided spinal anesthesia using the SonixGPS ultrasound guidance system: A feasibility study," *Acta Anaesthesiol. Scand.*, vol. 58, no. 7, pp. 875-881, 2014.

[94] F. Shen *et al.*, "Three-Dimensional Sonography With Needle Tracking," *J. Ultrasound Med.*, vol. 27, no. 6, pp. 895-905, 2008.

[95] I. Vesely *and W. Smith*, "Method for carrying out a medical procedure using a three-dimentional tracking and imaging system," 5,797,849, 1998.

[96] A. Krieger, R. C. Susil, G. Fichtinger, E. Atalar, and L. L. Whitcomb, "Design of a novel MRI compatible manipulator for image guided prostate intervention," in *Proceedings - IEEE International Conference on Robotics and Automation*, vol. 1, pp. 377-382, 2004.

[97] E. Yeniaras, Z. Deng, M. A. Syed, M. G. Davies, and N. V. Tsekos, "A novel virtual reality environment for preoperative planning and simulation of image guided intracardiac surgeries with robotic manipulators," in *Studies in Health Technology and Informatics*, vol. 163, pp. 716-722, 2011.

[98] C. M. Schneider, A. M. Okamura, and G. Fichtinger, "A robotic system for transrectal needle insertion into the prostate with integrated ultrasound," in *Proceedings - IEEE International Conference on Robotics and Automation*, vol. 1, pp. 365-370, 2004.

[99] A. Fenster, J. Bax, H. Neshat, D. Cool, N. Kakani, and C. Romagnoli, "3D ultrasound imaging in image-guided intervention," *36th Annual International Conference of the IEEE Engineering in Medicine and Biology Society, EMBC*, pp. 6151-6154, 2014.

[100] B. Konh, N. V. Datla, and P. Hutapea, "Analysis driven design optimization of sma-based steerable active needle," in *ASME 2014 Conference on Smart Materials, Adaptive Structures and Intelligent Systems, SMASIS*, pp. 1-6, 2014.

[101] T. Bruns *et al.*, "Design of an Autoclavable Active Cannula Deployment Device," *J. Med. Device.*, vol. 5, no. 2, pp. 1-5, 2011.

[102] R. J. Webster, J. Memisevic, and A. M. Okamura, "Design considerations for robotic needle steering," in *Proceedings - IEEE International Conference on Robotics and Automation*, pp. 3588-3594, 2005.

[103] M. Scali, T. P. Pusch, P. Breedveld, and D. Dodou, "Needle-like instruments for steering through solid organs: A review of the scientific and patent literature," *Proc. Inst. Mech. Eng. Part H J. Eng. Med.*, vol. 231, no. 3, pp. 250–265, 2017.

[104] "PROTOLABS." [Online]. Available: https://www.protolabs.com/materials/comparison-guide/.

[105] "Stratasys." [Online]. Available: https://www.stratasys.com/3d-printers/objet-350-500-connex3.

[106] O. Gerovichev, P. Marayong, and A. M. Okamura, "The effect of visual and haptic feedback on manual and teleoperated needle insertion," in *Lecture Notes in Computer Science*, pp. 147-154, 2002.

[107] B. MAURIN *et al.*, "IN VIVO STUDY OF FORCES DURING NEEDLE INSERTIONS," *Perspective in Image-Guided Surgery*, pp. 415-122, 2004.

[108] "VELMEX." [Online]. Available: https://www.velmex.com/Products/Controls/Motors.html.

[109] J. A. Bell *et al.*, "A deflectable guiding catheter for real-time MRI-guided interventions," *J. Magn. Reson. Imaging*, vol. 35, no. 4, pp. 908-915, 2012.

[110] B. Konh, N. V. Datla, and P. Hutapea, "Feasibility of Shape Memory Alloy Wire Actuation for an Active Steerable Cannula," *J. Med. Devices, Trans. ASME*, vol. 9, no. 2, pp. 1-2, 2015.

[111] S. Karimi and B. Konh, "3D Steerable Active Surgical Needle," *Design of Medical*

Devices, 2019.

[112] B. Konh, S. Karimi, and S. Miller, "Feasibility study of an active soft catheter actuated by SMA wires," *SPIE Smart Structures and Materials + Nondestructive Evaluation and Health Monitoring*, pp. 1-5, 2018.

[113] "MITSUMI Stepper Motor." [Online]. Available: https://www.mitsumi.co.jp/latest/Catalog/compo/motor/m25sp5_e.html.

[114] T. Lewis, "5 Fascinating Facts About Fetal Ultrasounds." [Online]. Available: https://www.livescience.com/32071-history-of-fetal-ultrasound.html.

[115] W. Xia *et al.*, "Looking beyond the imaging plane : 3D needle tracking with a linear array ultrasound probe," *Sci. Rep.*, vol. 7, no. 1, pp. 1–9, 2017.

[116] "Digital Color Doppler Ultrasound System," 2014. [Online]. Available: https://www.secma.se/wp-content/uploads/2012/12/ECO5-User-Manual_GB.pdf.

[117] T. Uematsu, M. Kasami, and Y. Kiyohara, "B-Mode Ultrasound Imaging, Doppler Imaging, and Real-Time Elastography in Cutaneous Malignant Melanoma and Lymph Node Metastases," *healthcare*, vol. 1, no. 1, pp. 84–95, 2013.

[118] Y. Lee, J. Kang, and Y. Yoo, "Automatic dynamic range adjustment for ultrasound B-mode imaging," *Ultrasonics*, vol. 56, pp. 435–443, 2015.

[119] A. Leibinger *et al.*, "Soft Tissue Phantoms for Realistic Needle Insertion," in *Annals of Biomedical Engineering*, vol. 44, no. 8, pp. 2442–2452, 2016.

[120] Y. Jheng and C. Lin, "Fabrication and Testing of Breast Tissue-Mimicking Phantom for Needle Biopsy Cutting," *Design of MEdical Devices*, pp. 1-2, 2017.

[121] M. S. Ju, H. M. Vong, C. C. K. Lin, and S. F. Ling, "Development of Soft Tissue Stiffness Measuring Device for Minimally Invasive Surgery by using Sensing Cum Actuating Method," in *ICMBE*, vol. 23, pp. 291–295, 2009.

[122] H. Oflaz and O. BARAN, "A new medical device to measure a stiffness of soft materials," *Acta of Bioengineering and Biomechanics*, vol. 16, no. 1, pp. 125-131, 2014.

[123] "Moulding Your Own Worms, Web Page." [Online]. Available: https://www.tacklecrafting.com/baits/pour_your_own_worms/.

[124] Z. Khashei Varnamkhasti, B. Konh, O. Haji Maghsoudi, Y. Yu, and L. Liao, "Ultrasound Needle Tracking Inside a Soft Phantom and Methods to Improve the Needle Tip Visualization," *Design of Medical Devices*, pp. 1-6, 2019.

[125] Z. Khashei Varnamkhasti and B. Konh, "Design and Performance Study of a Novel Minimally Invasive Active Surgical Needle," *J. Med. Device.*, 2019.

[126] N. V. Datla *et al.*, "Towards a nitinol actuator for an active surgical needle," in

ASME 2012 Conference on Smart Materials, Adaptive Structures and Intelligent Systems, SMASIS, pp. 265-269, 2012.

[127] Z. Wang, G. Hang, J. Li, Y. Wang, and K. Xiao, "A micro-robot fish with embedded SMA wire actuated flexible biomimetic fin," *Sensors Actuators, A Phys.*, vol. 144, no. 2, pp. 354-360, 2008.

[128] "RIGOL." [Online]. Available: https://www.rigolna.com/products/dc-power-loads/dp800/dp832/.

[129] M. Najafi and R. Rohling, "Single camera closed-form real-time needle trajectory tracking for ultrasound," *Proceedings of SPIE*, pp. 1-7, 2011.

[130] E. Ayvali and J. P. Desai, "Optical Flow-Based Tracking of Needles and Needle-Tip Localization Using Circular Hough Transform in Ultrasound Images," *HHS Public Access*, vol. 43, no. 8, pp. 1828-1840, 2015.

[131] Y. Zhao, A. Bernard, C. Cachard, and H. Liebgott, "Biopsy needle localization and tracking using ROI-RK method," *Abstr. Appl. Anal.*, pp. 1-7, 2014.

[132] O. H. Maghsoudi, A. Vahidpour Tabrizi, B. Robertson, and A. Spence, "Superpixels Based Marker Tracking Vs . Hue Thresholding In Rodent Biomechanics Application," *51st Asilomar Conference on Signals, Systems, and Computers*, pp. 209-213, 2017.

[133] O. H. Maghsoudi, A. Vahedipour, B. Robertson, and A. Spence, "Application of Superpixels to Segment Several Landmarks in Running Rodents," *Pattern Recognit. Image Anal.*, vol. 28, no. 3, pp. 468-482, 2018.